Network models of fluid, hexatic and polymerized membranes

1997 J. Phys.: Condens. Matter 9 8795

(http://iopscience.iop.org/0953-8984/9/42/001)

J. Phys.: Condens. Matter **9** (1997) 8795–8834. Printed in the UK PII: S0953-8984(97)72180-5

REVIEW ARTICLE

Network models of fluid, hexatic and polymerized membranes

G Gompper† and D M Kroll‡

† Max-Planck-Institut für Kolloid- und Grenzflächenforschung, Kantstrasse 55, 14513 Teltow, Germany

‡ Department of Medicinal Chemistry and Minnesota Supercomputer Institute, University of Minnesota, 308 Harvard Street SE, Minneapolis, MN 55455, USA

Received 9 June 1997

Abstract. The thermal behaviour of membranes—surfaces of nearly vanishing tension—depends strongly on their internal state, which can be either fluid, crystalline (or polymerized), or hexatic. Thermal fluctuations have a dramatic effect on the conformation and elastic properties of membranes. We describe in this review both the continuum models of membranes which are used for theoretical analyses as well as the network models employed in simulations. The fruitful interaction between these two approaches, which has lead to recent progress in this field, is emphasized. We summarize the essential results of recent research on fluctuating membranes; in particular, the effects of bending rigidity, self-avoidance, attractive interactions, disorder, topological defects and external compression forces are discussed in detail.

1. Introduction

Amphiphiles and lipids in aqueous solution self-assemble into a large variety of phases (Gompper and Schick 1994, Gelbart *et al* 1995). The driving force for structure formation in these systems is the hydrophobic effect—the hydrocarbon tail of an amphiphilic molecule wants to avoid contact with water or the polar heads of other amphiphiles—together with frustration—the polar head of an amphiphile is permanently linked to its tail, and cannot be separated from it in space (Tanford 1980, Israelachvili 1992). There are two principal ways to arrange amphiphilic molecules so that their hydrocarbon tails are shielded from water contact by a shell of polar head groups: spherical or cylindrical micelles, and bilayers. These structural elements can then assemble in different ways on larger length scales to form thermodynamically stable phases, such as the lamellar phase or the cubic bicontinuous gyroid phase (both of which are arrangements of bilayers).

In some cases, lamellar (Strey *et al* 1990) and cubic bicontinuous (Peter *et al* 1996) phases can be swollen enormously by adding water to the system. Inter-membrane separations on the order of several thousand ångströms—which is much greater than a typical bilayer thickness of some 10 Å—have been observed. Giant lipid bilayer vesicles with a typical size of 10 μm can also be made which are metastable over typical experimental timescales; the relative stability of these vesicles is due to the extremely small molecular solubility of the lipid molecules in water (Bloom *et al* 1991, Lipowsky and Sackmann 1995). In all of these cases, the relevant degrees of freedom of the system are the local positions of the amphiphilic bilayers—or membranes. The area of a membrane is determined by a balance of the hydrophobic energy, which arises from local hydrocarbon–water contact,

0953-8984/97/428795+40$19.50

and head–head and tail–tail repulsion. Due to this self-adjustment of the membrane area, shapes and fluctuations of *fluid* membranes are controlled by the curvature energy (Canham 1970, Helfrich 1973, Evans 1974).

More generally, membranes are two-dimensional sheets of molecules different from the medium in which they are embedded. Red-blood-cell cytoskeletons (Schmidt *et al* 1993, Elgsaeter *et al* 1986) provide an example of surfaces with fixed internal connectivity. Because of the fixed connectivity, this class of membrane has a finite shear modulus, so the shape and fluctuation spectra of these surfaces are controlled be a delicate interplay between the bending energy and in-plane elastic energy. Other examples of crystalline (or *polymerized*) membranes are graphite oxide sheets (Wen *et al* 1992, Spector *et al* 1994) and the surfaces of high-molecular-weight fullerenes (Lamb *et al* 1992).

At sufficiently low temperatures, amphiphilic bilayer membranes freeze. When confined to two dimensions, these surfaces exhibit quasi-long-range crystalline order, just like polymerized membranes. However, if they are allowed to buckle out of the plane, dislocations destroy the crystalline order at any finite temperature, resulting in a membrane with *hexatic* order (Nelson and Peliti 1987, Nelson 1996). The free energy and fluctuation spectra of this class of membrane are different from those of either fluid or polymerized membranes.

In this review, we attempt to summarize the essential results of recent research involving continuum models and simulations of network models of fluctuating membranes. As a consequence, we will mention work involving plaquette models defined on cubic lattices only very briefly. A nice review of random-surface models from the viewpoint of a high-energy physicist has appeared recently (Wheater 1994). Various related and complementary aspects of the physics of membranes are discussed in the recent reviews by Nelson *et al* (1989), Helfrich (1990), Lipowsky (1991), Grest and Murat (1995), Lipowsky and Sackmann (1995), David *et al* (1996) and Seifert (1997).

2. Continuum theory of membranes

Intermolecular interactions in membranes can be separated into two groups: (i) strong bonds between neighbouring particles in the network; and (ii) weaker van der Waals, hydrogen-bonding, and hard-core interactions between all of the particles in the network. The second class of interactions becomes important when particles that are distant neighbours along the membrane are actually close in real space.

2.1. Tethered networks

Consider first the contributions from the strong nearest-neighbour bonds that hold the network together. For a coarse-grained description of the network, the positions $\boldsymbol{r}_i$ of the individual particles are replaced by a coarse-grained average coordinate vector $\boldsymbol{r}(\boldsymbol{x})$ which is a function of the continuous *internal* coordinate $\boldsymbol{x}$ of particles in the network. The *external* coordinate $\boldsymbol{r}$ is the coarse-grained average of the positions of particles in the vicinity of point $\boldsymbol{x}$ in the network.

The form of the Landau–Ginzburg free-energy functional, $\mathcal{F}$, which describes the energy of an arbitrary configuration of the network, is dictated by symmetry considerations. The basic symmetries are invariance with respect to translations and rotations. The first implies that $\mathcal{F}$ can only depend on derivatives such as $\partial_\alpha \boldsymbol{r} \equiv \partial \boldsymbol{r}/\partial x_\alpha$ and $\partial_\alpha \partial_\beta \boldsymbol{r}$, while the second requires that all terms consist of scalar products of the form $\partial_\alpha \boldsymbol{r} \cdot \partial_\beta \boldsymbol{r}$. For an isotropic network, an expansion in powers of $\partial_\alpha \boldsymbol{r}$ yields the free-energy

functional (Paczuski *et al* 1988)

$$\mathcal{F}_1 = \int \mathrm{d}^D x \ \left[\frac{t}{2}(\partial_\alpha \boldsymbol{r})^2 + u(\partial_\alpha \boldsymbol{r} \cdot \partial_\beta \boldsymbol{r})^2 + v(\partial_\alpha \boldsymbol{r} \cdot \partial_\alpha \boldsymbol{r})^2 + \frac{\kappa}{2}(\partial_\alpha^2 \boldsymbol{r})^2 + \cdots \right] \tag{1}$$

where $D = 2$, $\alpha = 1, 2$ for membranes, and summation over repeated indices is implied. The terms in equation (1) have simple physical interpretations. The first, with coefficient t, represents a Hookean elasticity, while the terms with coefficients u and v are anharmonic elastic terms. The last term is a bending energy that arises from bond-bending forces. The coefficient κ is the bending rigidity. Both in-plane elasticity and bending rigidity are macroscopic manifestations of the internal connectivity.

In the subsequent discussion, it is often useful to consider the generalization of equation (1) to D-dimensional networks embedded in d-dimensional space. In this case, $\boldsymbol{r}$ is a d-dimensional vector, and $\alpha = 1, 2, \ldots, D$. For example, $D = 1$ corresponds to a linear molecule such as a polymer, and for $D = 3$, the model describes a gel. Non-integer D might approximate fractal structures.

Because the entropy-generated elastic energy of the network is minimized when it has a small size R in space, surface elements, or particles, that are distant neighbours along the network backbone can be in close physical contact. Their interaction can then no longer be ignored. At high temperatures, the particles only feel the hard-core interactions, which can be described by an interaction potential of the form $\frac{1}{2}b(T)\int \mathrm{d}^D x \ \int \mathrm{d}^D y \ \delta^{(d)}[\boldsymbol{r}(\boldsymbol{x}) - \boldsymbol{r}(\boldsymbol{y})]$. As in polymers, the coefficient $b(T)$ is related to the second virial coefficient in a solution of such networks, and can change sign as a function of the thermodynamic fields, such as temperature. Higher-order terms are then necessary to stabilize the system. Their contribution, $\mathcal{F}_2$, to the free energy functional is (Paczuski *et al* 1988)

$$\mathcal{F}_2 = \frac{1}{2}b(T)\int \mathrm{d}^D x_1 \int \mathrm{d}^D x_2 \ \delta^{(d)}[\boldsymbol{r}(\boldsymbol{x}_1) - \boldsymbol{r}(\boldsymbol{x}_2)] + c(T)\int \mathrm{d}^D x_1 \int \mathrm{d}^D x_2 \int \mathrm{d}^D x_3 \ \delta^{(d)}[\boldsymbol{r}(\boldsymbol{x}_1) - \boldsymbol{r}(\boldsymbol{x}_2)]\delta^{(d)}[\boldsymbol{r}(\boldsymbol{x}_2) - \boldsymbol{r}(\boldsymbol{x}_3)]. \tag{2}$$

The probability of a particular configuration of the network is determined by the free energy $\mathcal{F} = \mathcal{F}_1 + \mathcal{F}_2$.

The scaling behaviour can be studied using a Flory-type (mean-field) approximation. Consider a network of linear dimension L and let R be its size in space. In $\mathcal{F}_1$, we approximate terms of the type $\partial_\alpha r_i$ by R/L, and $\int \mathrm{d}^D x$ by L^D. In $\mathcal{F}_2$, the fact that $\int \mathrm{d}^d R \ \delta^{(d)}(\boldsymbol{R}) = 1$ suggests approximating $\delta^{(d)}(R)$ by R^{-d}. These estimates lead to the free-energy estimate (Paczuski *et al* 1988)

$$\mathcal{F} \sim tR^2L^{D-2} + wR^4L^{D-4} + \kappa R^2L^{D-4} + bL^{2D}/R^d + cL^{3D}/R^{2d} \tag{3}$$

where $w = u + Dv$. Since b and t can change sign with temperature, the terms with $c > 0$ and $w > 0$ are necessary to ensure stability.

A detailed discussion of the predictions of this approach is provided by Paczuski *et al* (1988) and Nelson (1989). Here we only consider the most important cases.

2.1.1. The crumpled phase. Both t and b are positive at sufficiently high temperatures; in this case, these two terms asymptotically dominate the rest. Minimizing equation (3) with respect to R, one finds

$$R \sim (b/t)^{1/(d+2)}L^{(D+2)/(d+2)}. \tag{4}$$

This corresponds to a *crumpled* network with a non-trivial fractal (or Haussdorf) dimension. Generally, a scaling exponent ν defined by the relation

$$R \sim L^{\nu} \tag{5}$$

is used to characterize the extent to which a D-dimensional network is crumpled in the d-dimensional embedding space. Alternatively, one can use the fractal dimension d_f which relates the mass ($\sim L^D$) of the network to its spatial extent:

$$L^D \sim R^{d_f} \tag{6}$$

to characterize the conformation. The relationship between these two exponents is $\nu = D/d_f$. The Flory estimate (4) for ν in this case is, therefore,

$$\nu_f = (D+2)/(d+2) \tag{7}$$

and

$$d_f = \frac{(d+2)D}{(D+2)}. \tag{8}$$

2.1.2. The flat phase. Result (4) indicates that R diverges for $t \to 0$. For $t < 0$, the anharmonic term wR^4L^{d-4} is needed for stability. The competition between these two terms leads to $R \sim |t|^{1/2}L$, which clearly describes an expanded *flat* phase.

2.1.3. The compact, collapsed phase. Equation (4) also predicts that $R \to 0$ as $b \to 0$. In this case, the three-body interaction with $c > 0$ is required for stability. It follows that

$$R \sim (c/|b|)^{1/d} L^{D/d} \tag{9}$$

for $b < 0$. This corresponds to a *compact*, or collapsed, structure. Although this compact structure minimizes the free energy, it is not clear that it is dynamically accessible. In addition, the competition between the attractive and repulsive inter-particle interaction can no longer be ignored, and the configuration landscape could be quite complicated.

2.1.4. The crumpling transition. The transition at $t = 0$ between the flat and the crumpled phases is called the *crumpling transition*. Assuming that both b and w are positive, one finds that

$$R \sim (b/w)^{1/(d+4)} L^{\nu_c}$$

with $\nu_c = (D+4)/(d+4)$ at the transition. Paczuski *et al* (1988) have shown that the distinct scaling forms in the vicinity of the crumpling transition can be combined into a single homogeneous scaling function

$$R \sim L^{\nu_c} \Psi(tL^y)$$

where $\Psi(0) =$ constant and $\Psi(x) \to |x|^{\phi_\pm}$ for $x \to \pm\infty$, with $y = 2(d-D)/(d+4)$, $\phi_- = 1/2$, and $\phi_+ = -1/(d+2)$. While different crossover exponents y_+ and y_- cannot be ruled out in general, they are the same in the present mean-field analysis.

2.1.5. Phantom networks and the influence of self-avoidance. Finally, if we ignore the interaction terms in $\mathcal{F}_2$ and assume $t > 0$, we have what is commonly called a *phantom* membrane in which the configurational free energy is determined by a network of Hookean springs which is allowed to self-intersect. This model is exactly soluble, and it is easy to see that

$$R \sim \begin{cases} L^{(2-D)/2} & \text{for } D < 2 \\ \{\ln(L)\}^{1/2} & \text{for } D = 2. \end{cases} \tag{10}$$

For $D > 2$, fluctuations are too weak to prevent the complete collapse of the network. Result (10) can also be obtained by either requiring that the Hookean term in equation (3), $R^2 L^{D-2}$, is of order one, or by dimensional analysis of the Gaussian free-energy functional. Assume now that R scales as in equation (10), and consider the scaling behaviour of the interaction term proportional to b in $\mathcal{F}_2$. One finds that this term scales as

$$L^{2D}/R^d \sim L^{2D-d(2-D)/2}. \tag{11}$$

The exponent on the right-hand side of this equation vanishes at the *upper critical dimension* (Kardar and Nelson 1987, Duplantier 1987, Aronowitz and Lubensky 1987),

$$d_{uc} = 4D/(2 - D). \tag{12}$$

This term is *irrelevant*, i.e. it scales to zero in the limit of large system sizes if $d > d_{uc}$; the scaling behaviour of the network is not changed by self-avoidance in this case. For polymers ($D = 1$), $d_{uc} = 4$. For numbers of dimensions greater than four, the conformation of a polymer is therefore described by the random-walk exponent $\nu = 1/2$. For $d = 3$, the Flory result (7) is an excellent approximation to the true scaling behaviour. For two-dimensional tethered networks, however, self-avoidance can only be neglected when $d = \infty$, in agreement with the fact that the fractal dimension of the non-interacting surface is infinite (Gross 1984). In view of this result, and the quality of the Flory approximation for polymers, one might expect that expression (4), with $D = 2$, would provide a reasonably accurate description of the scaling behaviour of self-avoiding tethered networks. As we shall see later, this is not the case. It is worth noting that if we assume the Flory scaling relation (4), n-body interactions are *relevant* for

$$d < \frac{2nD}{2(n-1) - D}. \tag{13}$$

For polymers, it follows that three-body interactions are relevant only for dimensions $d < 2$. In contrast, for $D = 2$, three-body terms are relevant below six dimensions, and four-body terms are relevant below four dimensions. In fact, for $d = 3$, three-, four-, and five-body interactions are all relevant, and six-body terms are marginal. All of these interaction terms can be expected to influence the scaling behaviour of the surface for $d = 3$ and need to be treated self-consistently (Hwa 1990, Grest 1991).

2.1.6. Polymeric fractals. Polymers and tethered membranes are special cases of more general *homogeneous* manifolds characterized by the parameter D. In view of the drastic differences between the conformation and phase behaviour of polymers ($D = 1$) and membranes ($D = 2$), it would be extremely useful to have realizations of networks characterized by $1 < D < 2$. While not homogeneous, regularly connected fractal networks (or polymeric fractals) are useful generalizations to consider (Cates 1984, Grest and Murat 1990, Levinson 1991, Grest and Murat 1995). These networks are characterized by a spectral dimension (Alexander 1982), d_s, which describes the intrinsic connectivity of the network,

and in many ways plays the role of D. Examples of polymeric fractals include linear polymers, swollen gelation/percolation clusters generated near the percolation threshold, Sierpinski gaskets, and branched polymers.

The spectral dimension can be defined in terms of the low-energy scaling behaviour of the density of states, $\mathcal{N}(E) \sim E^{d_s/2-1}$, of the Laplacian on the fractal. It also relates the mean square displacement in the embedding space of a random walk on the fractal to the time t (Gefen *et al* 1983),

$$\langle |\boldsymbol{r}(t) - \boldsymbol{r}(0)|^2 \rangle \sim t^{d_s/d_f} \tag{14}$$

where d_f is the fractal dimension of the network.

The mean-field analysis of the previous subsections can be easily extended to polymeric fractals. For a fractal generated on a lattice, the lattice fractal dimension d_{fl} relates the linear lattice size L_0 to the total number of nodes, N, by (Cates 1984)

$$N \sim L_0^{d_{fl}}. \tag{15}$$

Replace now every bond in the fractal by an identical section of ideal phantom polymer chain, and allow the network to relax off the lattice. This is the polymeric fractal. In general, the network will have a new internal size L; the relation between L and L_0 follows from simple mode counting: since $L^{d_s} \propto N$, it follows from equation (15) that $L^{d_s} \sim L_0^{d_{fl}}$.

Replacing D by d_s in equation (3), one finds, in analogy to equation (10), that for the phantom polymeric fractal, $R \sim L^{(2-d_s)/2} \sim N^{(2-d_s)/2d_s}$, so the fractal dimension is (Cates 1984)

$$d_{f_0} = 2d_s/(2 - d_s) \tag{16}$$

and the upper critical dimension

$$d_{uc} = 4d_s/(2 - d_s). \tag{17}$$

Similarly, in the crumpled phases, for $t > 0$ and $b > 0$,

$$R \sim (b/t)^{1/(d+2)} L^{(d_s+2)/(d+2)} \sim N^{1/d_f} \tag{18}$$

with

$$d_f = \frac{(d+2)d_s}{(d_s+2)} \tag{19}$$

in analogy with the result (8) for D-dimensional homogeneous manifolds. Flory theory therefore implies that the fractal dimension of the crumpled polymeric fractal depends only on the network connectivity, as described by d_s, and the spatial dimension d. It follows from equation (19) that Flory theory predicts that n-body interaction terms are relevant for $d < 2nd_s/[2(n-1) - d_s]$ (Grest 1991, Grest and Murat 1995).

2.1.7. Fluctuations and the crumpling transition. So far, we have not discussed the influence of critical fluctuations on the crumpling transition. Paczuski *et al* (1988) have shown that there is a mean-field crumpling transition of the type described in section 2.1.4 for all $D > D_c = 4$. They treated critical fluctuations in an expansion in $4 - D$; for $D \lesssim 4$, there is a second-order critical transition for $d > d_c(D) \approx 219 + \mathrm{O}(4 - D)$, while for $d < d_c$, there is a fluctuation-driven first-order transition. On the other hand, first-order expansions in $1/d$ (David and Guitter 1988, Aronowitz *et al* 1989) suggest that the transition is continuous. At the transition, $1/d$ expansions predict that $d_f = 3$. More recently, Le Doussal and Radzihovsky (1992) used a self-consistent screening approximation to study D-dimensional tethered networks embedded in d dimensions. The method is exact for large

d to order $1/d$, for any d to order $\epsilon = 4 - D$, and for $d = D$. For $D = 2$, $d = 3$, they find $d_f \approx 2.73$ at the crumpling transition.

The crumpling transition is analogous to transitions in magnetic systems with O(N) symmetry; the normal vectors of the membrane are the analogue of the spins of the magnetic system, and the dimension d of the embedding space corresponds to the number of components N of the spin vector. There is, however, a significant difference between the present problem and O(N) magnetic systems: the lower critical dimension of tethered membranes is less than two (Aronowitz *et al* 1989). A crumpling transition therefore occurs here in a two-dimensional system despite the Mermin–Wagner theorem. The reason for this breakdown of rotational symmetry is the existence of long-range forces mediated by phonons (Nelson and Peliti 1987). A related feature of this system is that anharmonicities in the flat phase lead to a breakdown of harmonic elasticity for all membrane dimensions D less than the upper critical dimension $D_c = 4$ (Aronowitz *et al* 1989).

2.1.8. Fluctuations about the flat phase. Fluctuations in the ordered, flat phase can be studied in an expansion about the flat state by introducing in-plane phonon modes u_α ($\alpha = 1, \ldots, D$) and out-of-plane undulation modes h_a ($a = D + 1, \ldots, d$) and setting (Paczuski *et al* 1988)

$$\boldsymbol{r}(\boldsymbol{x}) = m(x_\alpha - u_\alpha)\boldsymbol{e}_\alpha + h_a \boldsymbol{e}_a. \tag{20}$$

The $\{\boldsymbol{e}_\alpha\}$ are a set of orthonormal in-plane basis vectors, and $\{\boldsymbol{e}_a\}$ are a set of orthonormal basis vectors in the subspace normal to the plane of the network. To leading order in gradients of u_α and h_a, the free energy (1) reduces to

$$\mathcal{F} = \int \mathrm{d}^D x \left[\frac{1}{2}\kappa(\nabla^2 \boldsymbol{h})^2 + \mu u_{\alpha\beta}^2 + \frac{1}{2}\lambda u_{\gamma\gamma}^2 \right] \tag{21}$$

where $u_{\alpha\beta} = [\partial_\alpha u_\beta + \partial_\beta u_\alpha + \partial_\alpha \boldsymbol{h} \cdot \partial_\beta \boldsymbol{h}]/2$ is the strain matrix, and the elastic constants are $\mu = 4um^4$ and $\lambda = 8vm^4$. Here and in the following, we measure all energies in units of $k_B T$.

Nelson and Peliti (1987) have shown that the long-range orientational order which occurs in $D = 2$ networks at large bending rigidities is due to a long-range interaction between local Gaussian curvatures mediated by transverse phonons of the crystalline membrane. Using a simple one-loop self-consistent theory for $D = 2$, *assuming* non-vanishing elastic constants, they showed that phonon-mediated interactions between capillary waves lead to a renormalization, or wavevector dependence of the bending rigidity of the form

$$\kappa(q) \sim q^{-\eta} \tag{22}$$

with $\eta = 1$. The theory of fluctuations about the flat phase was extended by Aronowitz and Lubensky (1988) to general D and d. An $\epsilon = 4 - D > 0$ expansion confirmed that the flat phase is described by non-trivial scaling behaviour, with $\kappa(q)$ scaling as in equation (22), but with *anomalous*, scale-dependent elastic constants

$$\lambda(q) \sim \mu(q) \sim q^{\omega} \tag{23}$$

with $\omega > 0$. It was also shown (Aronowitz and Lubensky 1988) that, as a consequence of rotational invariance,

$$\omega = 4 - D - 2\eta. \tag{24}$$

An explicit renormalization group calculation to first order in $\epsilon \equiv 4 - D$ yielded the result $\eta = 12(4 - D)/(24 + d - D)$. For flat, planar networks ($D = 2$, $d = 3$) this implies

$\eta = 24/25 = 0.96$. The Poisson ratio, $\sigma_p = \lim_{q\to 0} \lambda(q)/[\lambda(q) + 2\mu(q)]$, is predicted to be universal, with $\sigma_p = -1/5$, independent of both d and D.

More recently, Le Doussal and Radzihovsky (1992) used the self-consistent screening approximation, and found $\eta = 4/(1 + \sqrt{15}) \approx 0.821$ for $D = 2$ in three dimensions. This is currently the most accurate theoretical estimate for η. The Poisson ratio is predicted to be $\sigma_P = -1/3$.

The renormalized elastic constants enter an effective, long-wavelength free energy for the Fourier-transformed phonon, $\boldsymbol{u}$, and undulation, $\boldsymbol{h}$, modes. For the physically relevant case $D = 2$, $d = 3$, $\boldsymbol{u}$ is a two-dimensional vector, and h is a scalar. The effective free-energy functional for these modes is (Abraham and Nelson 1990b)

$$\mathcal{F}_{eff} = \int \frac{\mathrm{d}^2 q}{(2\pi)^2} \{\kappa(q) q^4 |h_q|^2 + \mu(q) q^2 |u_q|^2 + [\mu(q) + \lambda(q)] |\boldsymbol{q} \cdot \boldsymbol{u}_q|^2\}. \tag{25}$$

The size of the out-of-plane fluctuations in a network with a characteristic linear dimension L is

$$\langle h^2(\boldsymbol{x})\rangle \approx \frac{1}{2\pi} \int_{L^{-1}}^{a^{-1}} \frac{q\ \mathrm{d}q}{q^4 \kappa(q)} \sim L^{2\zeta} \tag{26}$$

where $\zeta = 1 - \eta/2$ and a is a short-distance cut-off of the order of the lattice spacing of the network. Similarly, the amplitudes of in-plane phonon fluctuations are given by $\langle |\boldsymbol{u}(\boldsymbol{x})|^2\rangle \sim L^{\omega}$.

The structure factor of an oriented tethered network is defined by (Abraham and Nelson 1990a)

$$S(q_z, q_\perp, L) = \frac{1}{N^2} \sum_{\boldsymbol{x},\boldsymbol{x}'} \langle \mathrm{e}^{\mathrm{i}\boldsymbol{q}\cdot[\boldsymbol{r}(\boldsymbol{x}) - \boldsymbol{r}(\boldsymbol{x}')]} \rangle = \frac{1}{N^2} \sum_{\boldsymbol{x},\boldsymbol{x}'} \langle \mathrm{e}^{\mathrm{i}q_z[r_z(\boldsymbol{x}) - r_z(\boldsymbol{x}')]} J_0(q_\perp |\boldsymbol{r}_\perp(\boldsymbol{x}) - \boldsymbol{r}_\perp(\boldsymbol{x}')|) \rangle \tag{27}$$

where $r_z(\boldsymbol{x})$ is the network coordinate along the direction of the smallest eigenvalue of the moment-of-inertia tensor and $\boldsymbol{r}_\perp(\boldsymbol{x})$ is the corresponding perpendicular component; the z-axis is aligned with the average normal to the surface. The brackets in equation (27) denote both a thermal average and an average over directions perpendicular to z. For an oriented membrane, it has been shown by Abraham and Nelson (1990a) that the structure function $S(q_z, 0, L)$ scales in qL^{ζ} for $q \lesssim 1/a$. For $q_z = 0$, however, there is a breakdown of scaling, and large in-plane phonon fluctuations cause $S(0, q_\perp, L)$ not to scale in $q_\perp L$ over a wide range of intermediate wavevectors.

Many laboratory experiments on tethered membranes are carried out on unoriented membranes. The scaling behaviour in this case has been analysed by Goulian *et al* (1992). It was shown that the orientationally averaged structure factor $S(q) \sim 1/q^2$ for small q. If the amplitudes of the longitudinal and transverse fluctuations are of the order of the inter-monomer distance a, this result holds for all $q \ll 1/a$, and $S(q)$ is indistinguishable from the structure factor for a randomly oriented flat plate. If the amplitudes of the longitudinal and transverse fluctuations are much larger than a, however, $S(q) \sim 1/q^2$ only for $q \ll 1/l$, where l depends on the amplitude of these fluctuations. The behaviour of the structure factor for $q \gg 1/l$ depends on the relative amplitude of the phonon and undulation modes. If in-plane fluctuations are small or absent, $S(q) \sim 1/q^{3-\zeta}$, while if their amplitude is large, $S(q) \sim 1/q^{4\zeta - 2}$.

For a crumpled membrane, the structure factor satisfies the scaling form $S(q, L) = S(qR_g) = S(qN^{1/d_f})$, where d_f is the fractal dimension of the network (Ceperley *et al* 1978, Kantor *et al* 1987). For intermediate q, $S(q) \sim 1/q^{d_f}$.

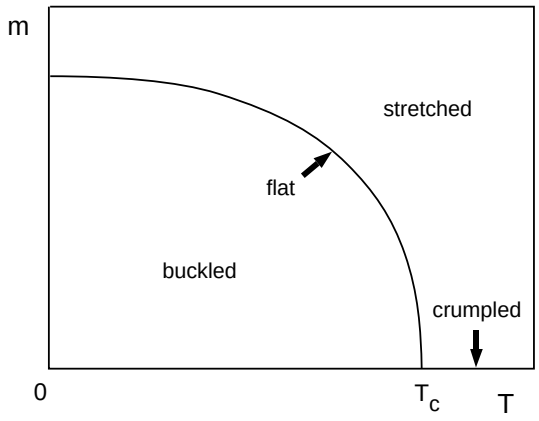

Figure 1. A schematic phase diagram of polymerized membranes in the (m, T) plane. The crumpling transition is located at $m = 0$, $T = T_c$.

2.1.9. Tension and the buckling transition. The results described in the previous two sections apply to unconstrained networks, such as those with free edges. However, membranes can be subjected to a large variety of boundary conditions. A simple generalization of the free-boundary case corresponds to suspending the network in a frame. A change of the size of the frame can induce a homogeneous tension or tangential pressure on the membrane (Guitter *et al* 1988, 1989, Aronowitz *et al* 1989, Guitter *et al* 1990). The resulting phase diagram is summarized in figure 1. The variable m measures the ratio of the linear size of the frame to the internal size L of the network at $T = 0$ without tension. For free boundary conditions, m has the value $m_{sp}(T)$, which is positive in the flat phase (for $T < T_c$) and zero for $T > T_c$. m_{sp} therefore serves as an order parameter for the crumpling transition. In analogy to standard critical phenomena, if the crumpling transition is continuous, the free energy should satisfy the scaling relation (Aronowitz *et al* 1989)

$$F(t, \sigma) = t^{2-\alpha}\Sigma(\sigma/t^{\Delta}) \tag{28}$$

where t is the reduced temperature, the 'tension' σ (defined by $\sigma = (1/L^D)\partial H/\partial m$, where H is the Helmholtz free energy of the membrane) is the field conjugate to the order parameter m, and Δ is the gap exponent. At the critical point,

$$m \sim \sigma^{1/\delta} \tag{29}$$

where $\delta = (D + 2 - \eta_c)/(D - 2 + \eta_c)$, and $\eta_c(D, d)$ is related to the fractal dimension at the crumpling transition by

$$\eta_c = [(4 - D)d_f - 2D]/d_f \tag{30}$$

for $D < 4$ (Aronowitz *et al* 1989). The region $m > m_{sp}$ corresponds to a stretched membrane which is under tension, and for $T < T_c$, m approaches m_{sp} as

$$m - m_{sp}(T) \sim \sigma^{1/\delta'} \tag{31}$$

for $\sigma \to 0$. Inside the coexistence region, $|m| < m_{sp}(T)$, the network buckles into an inhomogeneous mixed thermodynamic state consisting of a mixture of flat states with different orientations. Crossing the line $m = m_{sp}(T)$ corresponds to a *buckling transition* with one relevant scaling field. The exponent δ' in equation (31) can be expressed in terms of the exponent η of the flat phase as (Aronowitz *et al* 1989, Guitter *et al* 1989)

$$\delta' = (2 - \eta)/(D - 2 + \eta). \tag{32}$$

Since $\delta' \neq 1$, there is a breakdown of the linear Hooke's law relation between stress and strain.

2.2. Fluid membranes

The Hamiltonians of fluid membranes are invariant not only under rotations and translations, but also under reparametrizations. This additional invariance is due to the fluid structure, which does not allow a preferred coordinate system, and therefore cannot support shear stress. Fluid membranes are compressible, but the compressibility modulus is usually rather large, so they are often studied in the incompressible limit, where the membrane area is fixed. In this case, the only contribution to the configurational energy is the bending energy. For membranes which do not have a preferred radius of curvature, the curvature elastic energy has the form (Canham 1970, Helfrich 1973, Evans 1974)

$$\beta\mathcal{H}_b = \int \mathrm{d}S \left[\frac{1}{2}\kappa H^2 + \bar{\kappa} K\right] \tag{33}$$

where κ is the bending rigidity, $\bar{\kappa}$ the saddle-splay modulus, and H and K are the trace and determinant of the curvature tensor, respectively. For fixed topology, the second term in equation (33) is a constant, by the Gauss–Bonnet theorem. Morse and Milner (1995) have shown that a finite compressibility does not change the scaling behaviour; we therefore ignore compressibility effects in the following.

For the fluctuations of an almost spherical vesicle of radius r_0, the radial position vector of the vesicle at solid angle $\Omega \equiv (\theta, \phi)$ can be written as

$$r(\Omega) = r_0[1 + u(\Omega)] \tag{34}$$

where $u(\Omega)$ is the dimensionless amplitude of radial displacement. An expansion of u in spherical harmonics reads

$$u(\Omega) = \sum_{l=0}^{l_M} \sum_{m=-l}^{l} u_{lm} Y_{lm}(\Omega) \tag{35}$$

where l_M is a large wavenumber cut-off determined by the number of degrees of freedom; since only motion normal to the vesicle surface is relevant, $(l_M + 1)^2 = N$ in the present case. The excess bending energy $\Delta E \equiv (\kappa/2)[\int \mathrm{d}S\ H^2 - 16\pi]$, area A, and volume V of the vesicle can be written (to order u^2) as (Milner and Safran 1987, Helfrich 1986)

$$\Delta E = \frac{\kappa}{2} \sum_{l,m} |u_{lm}|^2 l(l+1)(l-1)(l+2) \tag{36}$$

$$A = 4\pi r_0^2 (1 + u_0)^2 + r_0^2 \sum_{l>0} |u_{lm}|^2 [1 + l(l+1)/2] \tag{37}$$

and

$$V = \frac{4\pi}{3} r_0^3 (1 + u_0)^3 + r_0^3 \sum_{l>0} |u_{lm}|^2 \tag{38}$$

where $u_0 = u_{00}/(4\pi)^{1/2}$.

The constant-area constraint is incorporated by choosing u_0 to satisfy $A = 4\pi r_0^2$, which implies

$$(1 + u_0)^2 = 1 - \frac{1}{4\pi} \sum_{l>0} |u_{lm}|^2 [1 + l(l+1)/2]. \tag{39}$$

The average volume of a fluctuating vesicle in this approximation is then given by

$$\langle V\rangle = V_0\left\{1+\frac{3}{8\pi\kappa}\sum_{l=2}^{l_M}\frac{(2l+1)[1-l(l+1)/2]}{l(l+1)(l-1)(l+2)}\right\} \tag{40}$$

where $V_0 = 4\pi r_0^3/3$. Both the effective radius $r_{eff} = r_0(1+u_0)$ and the average volume therefore depend *logarithmically* on the surface area (Gompper and Kroll 1996):

$$\langle r_{eff}\rangle/r_0 \approx 1-\frac{1}{4\pi\kappa}\ln(l_M/2) \tag{41}$$

$$\langle V\rangle/V_0 \approx 1-\frac{3}{8\pi\kappa}\ln(l_M/2) \tag{42}$$

where $l_M \sim \sqrt{A}$.

A systematic theory of vesicle fluctuations with several constraints, like fixed area *and* fixed volume, has been developed by Seifert (1995) (see also Seifert (1997)) and Heinrich *et al* (1997).

The interaction between the undulation modes leads to a renormalization of the bending rigidity (Helfrich 1985, Peliti and Leibler 1985, Cai *et al* 1994):

$$\kappa_R(\ell) = \kappa - \frac{\alpha_\kappa}{4\pi}\ln(\ell/a) \tag{43}$$

which *softens* the membrane on large length scales ℓ. Here, a is a microscopic length. The prefactor α_κ has been predicted to be universal. However, there has been a long-standing debate about its value; both $\alpha_\kappa = 3$ (Peliti and Leibler 1985, Förster 1986, Kleinert 1986, David and Leibler 1991, Cai *et al* 1994) and $\alpha_\kappa = 1$ (Helfrich 1985) have been suggested.

2.3. Hexatic membranes

The hexatic phase of planar membranes is characterized by short-range translational order, as in fluid membranes, and quasi-long-range bond-orientational order (Kosterlitz and Thouless 1973, Halperin and Nelson 1978, Young 1979). It is the bond-orientational order that distinguishes the hexatic from the fluid phase. In order to describe hexatic order, a set of orthonormal unit vectors $\boldsymbol{e}_1(\boldsymbol{x})$ and $\boldsymbol{e}_2(\boldsymbol{x})$ is introduced at each point of the surface. Hexatic order is then described by the local bond order parameter

$$\boldsymbol{m}(\boldsymbol{x}) = \cos\theta(\boldsymbol{x})\boldsymbol{e}_1 + \sin\theta(\boldsymbol{x})\boldsymbol{e}_2 = \sum_\alpha m_\alpha \boldsymbol{e}_\alpha \tag{44}$$

where $\theta(\boldsymbol{x})$ has sixfold symmetry. Since the hexatic order parameter $\boldsymbol{m}$ has a fixed magnitude, and there are no external fields aligning $\boldsymbol{m}$ along a particular direction, the lowest non-trivial contribution to the energy arises from its gradients (Nelson and Peliti 1987, David 1989, Park and Lubensky 1996c),

$$\mathcal{F}_A = \frac{1}{2}K_H\int \mathrm{d}S\; g^{ij}D_i\boldsymbol{m}\cdot D_j\boldsymbol{m} \tag{45}$$

where K_H is the hexatic stiffness, and D_i is the covariant derivative. In order to compare order parameters $\boldsymbol{m}(\boldsymbol{x})$ and $\boldsymbol{m}(\boldsymbol{x}')$ at two different points $\boldsymbol{x}$ and $\boldsymbol{x}'$, one has to parallel transport the order parameter at $\boldsymbol{x}$ along the geodesic to $\boldsymbol{x}'$. Under parallel transport in direction $\mathrm{d}x^i$, the unit vectors $\boldsymbol{e}_1$ and $\boldsymbol{e}_1$ are rotated by an angle $A_i\ \mathrm{d}x^i$; the covariant derivative is then given by

$$D_i m_\alpha = \partial_i m_\alpha + \epsilon_{\alpha\beta}A_i m_\beta \tag{46}$$

where $\epsilon_{\alpha\beta}$ is the antisymmetric tensor with $\epsilon_{12} = -\epsilon_{21} = 1$. The vector field A_i is the *spin connection*, whose curl is the Gaussian curvature,

$$\gamma^{ij}\,\partial_i A_j = K \tag{47}$$

where $\gamma^{ij} = \epsilon_{ij}/\sqrt{g}$. With the use of equation (46), the free energy (45) can finally be written as (Nelson and Peliti 1987, David 1989, Park and Lubensky 1996c)

$$\mathcal{F}_A = \frac{1}{2}K_H \int \mathrm{d}S\; g^{ij}(\partial_i\theta - A_i)(\partial_j\theta - A_j). \tag{48}$$

The excitations which destroy the hexatic order and cause a Kosterlitz–Thouless transition to the fluid phase are disclinations. They give rise to a singular contribution, θ_{dclin}, to the bond vector field; the disclination density, $s(\boldsymbol{x})$, is given by

$$s(\boldsymbol{x}) = \gamma^{ij}\,\partial_i\partial_j\theta_{dclin}. \tag{49}$$

The contribution of disclinations to the free energy (48) is (Park and Lubensky 1996a, c, Deem and Nelson 1996)

$$\mathcal{F}_C = -\frac{1}{2}K_H \int \mathrm{d}S\; (s-K)\frac{1}{\Delta_g}(s-K) \tag{50}$$

where $\Delta_g = D^i D_i$ is the Laplacian on the surface with metric tensor g_{ij}. Two conclusions can be drawn from this result. First, the relevant quantity is not the disclination density or the Gaussian curvature separately, but rather the difference between them. The disclination density can therefore be screened by the Gaussian curvature. Second, there is a long-range Coulomb interaction between the densities $(s(\boldsymbol{x}) - K(\boldsymbol{x}))$ at different parts of the surface.

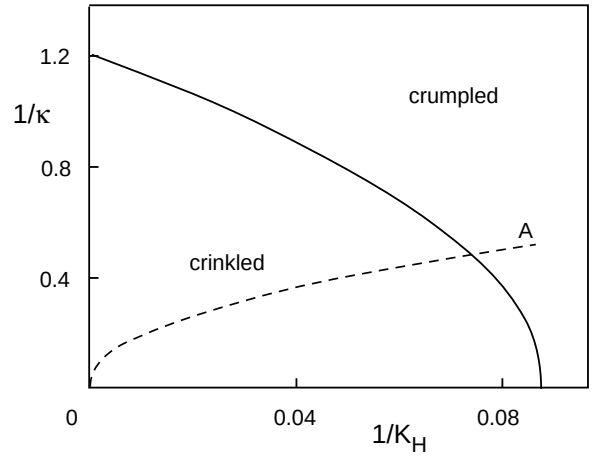

Figure 2. The phase diagram for hexatic membranes in the $(1/\kappa – 1/K_H)$ plane. The renormalization group calculations underlying this diagram are approximately valid below the line 0A. The crinkled-to-crumpled transition occurs via disclination melting in this case. Redrawn from Park and Lubensky (1996c).

The phase behaviour of this model has been studied in detail (Nelson and Peliti 1987, David *et al* 1987, Guitter and Kardar 1990, Park and Lubensky 1996a, b, c, Deem and Nelson 1996, Nelson 1996). The phase diagram which has now emerged, based on a careful renormalization group analysis (Park and Lubensky 1996c), is shown in figure 2. There is a hexatic, 'crinkled' phase, which is characterized by an *algebraic* decay of the correlation

function of surface normal vectors, at large bending rigidity κ and hexatic stiffness K_H. A Kosterlitz–Thouless transition to a fluid, 'crumpled' phase occurs not only with decreasing K_H, but *also* with decreasing κ.

It has been argued by Nelson (1996) that the free energies of isolated fivefold and sevenfold disclinations in hexatic membranes need not be identical. This asymmetry has been confirmed by explicit calculations of the shapes and energies of these disclinations (Park and Lubensky 1996a, Deem and Nelson 1996). However, this does *not* lead to two distinct Kosterlitz–Thouless defect proliferation temperatures in the thermodynamic limit—with periodic boundary conditions—since a 'charge-neutrality' condition dictates identical numbers of fivefold and sevenfold disclinations in this case. On the other hand, for membranes of finite size with free edges, the lower energy of fivefold disclinations indicates a tendency towards the formation of spherical vesicles (Nelson 1996, Deem and Nelson 1996); even in this case, however, it has been argued that in the basin of attraction of the hexatic fixed point, thermal fluctuations always drive the system into an 'unbuckled' regime, where disclinations proliferate at the same critical temperature (Deem and Nelson 1996).

3. Models of polymerized membranes

3.1. Tethered networks

Polymerized membranes can be modelled by a network of particles that are connected together to form a regular two-dimensional array embedded in $d = 3$ dimensions. While the network is generally taken to be a triangular array, the type of lattice is, to a large extent, unimportant (Baig *et al* 1994). Similarly, the exact form of the 'binding' potential between neighbouring particles is also irrelevant. However, it is essential that the bonds between adjacent particles cannot be broken so that the connectivity is fixed. This guarantees that the network has a finite shear modulus. Each particle or vertex is labelled by a two-dimensional *internal* coordinate vector $\boldsymbol{x} \equiv (x_1, x_2)$, with discrete x_1 and x_2, denoting its place in the network. For a triangular mesh, two primitive vectors $\{\boldsymbol{a}^{(1)}, \boldsymbol{a}^{(2)}\}$ of equal length ℓ_0 making an angle of 60° define the lattice. The locations of the vertices in the lattice are given by

$$\boldsymbol{x} = m\boldsymbol{a}^{(1)} + n\boldsymbol{a}^{(2)} \tag{51}$$

where m and n are integers. Two general classes of nearest-neighbour interaction potentials have been used in simulation studies of polymerized membranes. In the first, the vertices are point particles with harmonic nearest-neighbour interactions (Ambjørn *et al* 1989, Baig *et al* 1989a). In the second, hard spheres of radius σ_0 are placed at each vertex, and the spheres interact via tethers of maximum extension ℓ_0 (Kantor and Nelson 1987a). A variant of the tether-and-bead model, in which the hard-sphere and tethering potentials are replaced by anharmonic interaction potentials, is used in molecular dynamics (MD) simulations (Abraham *et al* 1989).

3.1.1. Tether-and-bead and Gaussian models. One of the simplest tethering potentials, $V(r)$, is one which causes the particles to behave as if tethered by a string,

$$V(r) = \begin{cases} 0 & \text{if } r < \ell_0 \\ \infty & \text{otherwise.} \end{cases} \tag{52}$$

The potential $V(r)$ acts only between tethered nearest neighbours; it ensures that the distance between nearest neighbours is less than ℓ_0. If this is the only interaction between particles,

we have a 'phantom' tethered surface which can self-intersect when large fluctuations bring distant segments of the network into close spatial proximity. Phantom membranes are very flexible surfaces, and there is no resistance to bending. They can roll up or collapse at no energy cost.

The total interaction energy of the network is

$$\beta E_{nn} = \sum_{\langle \boldsymbol{x}, \boldsymbol{x}' \rangle} V(|\boldsymbol{r}(\boldsymbol{x}) - \boldsymbol{r}(\boldsymbol{x}')|). \tag{53}$$

The thermal behaviour of the network can be determined exactly for the Gaussian potential $V(r) = (K_0/2)(r/a)^2$. In this case, the mean value of the mean square separation $|\boldsymbol{r}(\boldsymbol{x}) - \boldsymbol{r}(\boldsymbol{x}')|^2$ is (Kantor *et al* 1987)

$$\langle |\boldsymbol{r}(\boldsymbol{x}) - \boldsymbol{r}(\boldsymbol{x}')|^2 \rangle \simeq \frac{\mathrm{d}a^2}{\pi\sqrt{3}K_0} \ln(|\boldsymbol{x} - \boldsymbol{x}'|/a) \tag{54}$$

for $|\boldsymbol{r}(\boldsymbol{x}) - \boldsymbol{r}(\boldsymbol{x}')| \gg a$. The radius of gyration squared

$$R_G^2 = \frac{1}{2A^2} \int \mathrm{d}^2x \int \mathrm{d}^2x' \ \langle |\boldsymbol{r}(\boldsymbol{x}) - \boldsymbol{r}(\boldsymbol{x}')|^2 \rangle \tag{55}$$

where A is the area of the network therefore scales as $R_G^2 \sim \ln(L)$ with the linear size L of the membrane (see equation (10))—independently of the spatial dimension.

Simulations have shown that the same scaling behaviour is obtained for the tethering potential (52). Furthermore, a simple Migdal–Kadanoff bond-moving renormalization group approximation has been used (Kantor *et al* 1987) to show that potentials of this form are mapped into a Gaussian under iteration, supporting the view that the logarithmic scaling behaviour of the radius of gyration squared is universal for networks with central-force nearest-neighbour interactions. A related class of models with an elastic energy proportional to the sum of the areas of the elementary triangles have also been studied (Gross 1984, Billoire *et al* 1984). The results indicate that this model also belongs to the same universality class. However, as pointed out by Ambjørn *et al* (1985), this model has the pathology that the partition function is dominated by surfaces with infinite spikes in the thermodynamic limit. This happens because essentially all of the surface area is taken up by a small number of elementary surface triangles, with all others becoming vanishingly small. It is clear that models with the interaction energy (53) do not share this problem.

3.1.2. Self-avoidance. In simulations, self-avoidance can be guaranteed by placing a particle at each vertex which is large enough that it cannot pass through the network mesh. In Monte Carlo simulations, the particles are taken to be hard spheres of diameter σ_0. In this case, $V(r)$ is augmented by the potential

$$V_{HS}(r) = \begin{cases} \infty & \text{if } r < \sigma_0 \\ 0 & \text{otherwise} \end{cases} \tag{56}$$

between *all* beads. Self-avoidance requires $\ell_0/\sigma_0 < \sqrt{3}$. Since these potentials do not introduce an energy scale into the problem, the results are independent of temperature, and the free energy is solely due to entropic effects. Such potentials may be expected to generate small persistence lengths, and thus reduce the crossover effects (Kantor *et al* 1986). In molecular dynamics simulations, it is convenient to use a softer interaction potential, and a purely repulsive Lennard-Jones potential is generally used. For any of these choices, the long-wavelength elastic properties of the network should be similar to real polymerized membranes.

3.1.3. Bending energy. In Monte Carlo simulations, an explicit bending rigidity can be added using any of a number of discretizations of the bending energy of the membrane.

One commonly used discretization (Kantor and Nelson 1987a) of the bending energy is

$$\beta E_b^{norm} = \frac{1}{2}\lambda_b \sum_{\langle ij \rangle} |\boldsymbol{n}_i - \boldsymbol{n}_j|^2 = \lambda_b \sum_{\langle ij \rangle} (1 - \boldsymbol{n}_i \cdot \boldsymbol{n}_j) \tag{57}$$

where the sum runs over all pairs of neighbouring triangles, and $\boldsymbol{n}_i$ is the surface normal vector of triangle i. In the continuum limit, the difference $\boldsymbol{n}_i - \boldsymbol{n}_j$ becomes the gradient of the unit-normal vector field (Seung and Nelson 1988), and

$$\beta E_b^{norm} \rightarrow \beta \mathcal{H}_{norm} = \frac{1}{2}\kappa \int \mathrm{d}S \; g^{ij} \, \partial_i \boldsymbol{n} \cdot \partial_j \boldsymbol{n}_j \tag{58}$$

where g^{ij} is the contravariant metric tensor. Equation (58) is equivalent to the bending energy $\beta \mathcal{H}_b$, equation (33), with $\bar{\kappa} = -2\kappa$ (Seung and Nelson 1988). The relationship between the bending rigidity λ_b in equation (57) and κ can be determined by either discretizing equation (58) on a random surface, as described by Gompper and Kroll (1996) and Itzykson (1986), or by covering a sphere or cylinder with a number $N_\triangle$ of equilateral triangles and taking the limit $N_\triangle \rightarrow \infty$. Surprisingly, the result of the latter procedure depends on the shape of the surface! While both explicit discretization and coverings of a sphere yield $\lambda_b = \sqrt{3}\kappa$ (Kroll and Gompper 1992a, Gompper and Kroll 1996), coverings of a cylinder yield $\lambda_b = 2\kappa/\sqrt{3}$ (Seung and Nelson 1988, Gompper and Kroll 1996). This problem is discussed rather extensively by Gompper and Kroll (1996).

Discretizations of the squared Laplacian form of the bending energy

$$\beta \mathcal{H}_{Lap} = \int \mathrm{d}S \; (\Delta \boldsymbol{R})^2 \equiv \int \mathrm{d}S \; H^2 \tag{59}$$

do not share this pathology (Gompper and Kroll 1996). A general introduction to methods for discretizing operators on triangulated random surfaces is given by Itzykson (1986). On a triangulated surface, the mean curvature at node i is

$$H = \boldsymbol{n} \cdot \Delta \boldsymbol{R} \rightarrow H_i = \frac{1}{\sigma_i} \boldsymbol{n}_i \cdot \sum_{j(i)} \frac{\sigma_{ij}}{l_{ij}} (\boldsymbol{R}_i - \boldsymbol{R}_j) \tag{60}$$

where $\boldsymbol{n}_i$ is the surface normal at node i and the sum is over the neighbours of site i. l_{ij} is the distance between the two nodes i and j, σ_{ij} is the length of a bond in the dual lattice (Itzykson 1986), and

$$\sigma_i = \frac{1}{4} \sum_{j(i)} \sigma_{ij} l_{ij} \tag{61}$$

is the area of the virtual dual cell of vertex i. The length σ_{ij} in equations (60) and (61) is given by $\sigma_{ij} = l_{ij}[\cot(\theta_1) + \cot(\theta_2)]/2$, where θ_1 and θ_2 are the two angles opposite link ij in the triangles (ijk) and (ijk'), respectively. Note that since $\cot(\theta) < 0$ if θ is obtuse, σ_{ij}/l_{ij} can be negative if the sides of the two triangles are significantly different. Although there are some sum rules, such as $\sum_i \sigma_i = A$, where A is the area of the surface, there is no guarantee, in general, that the σ_{ij}, or even the σ_i, are positive (Itzykson 1986). While this causes no problems in simulation studies of the self-avoiding tether-and-bead models, it can in certain related models, where the vertices are point particles, and the nearest-neighbour interaction potential is harmonic (Espriu 1987, Baillie *et al* 1990).

Since $\boldsymbol{n} \parallel \Delta \boldsymbol{R}$ for surfaces embedded in three dimensions, equation (60) implies that the Laplacian squared bending energy can be written as (Itzykson 1986, Espriu 1987)

$$\beta E_b^{Lap} = \frac{\tau}{2} \sum_i \sigma_i (\Delta \boldsymbol{R})_i^2 = \frac{\tau}{2} \sum_i \frac{1}{\sigma_i} \left[\sum_{j(i)} \frac{\sigma_{ij}}{l_{ij}} (\boldsymbol{R}_i - \boldsymbol{R}_j) \right]^2 \tag{62}$$

with $\tau = \kappa$. Other discretizations of the bending energy which involve similar local averages of the mean curvature have been used by Gompper and Goos (1994) and Jülicher (1994).

In simulations performed using Gaussian spring models, the discretization (62) cannot be used, because there are large fluctuations in both the size and shape of the elementary triangles. In this case, some σ_i can be very small or negative, resulting in unphysical contributions to the bending energy. In this case, a simpler version of the bending energy (Espriu 1987, Baillie *et al* 1990),

$$\beta \tilde{E}_b^{Lap} = \frac{\tau}{2} \sum_i \frac{1}{\Omega_i} \left[\sum_{j(i)} (\boldsymbol{R}_i - \boldsymbol{R}_j) \right]^2 \tag{63}$$

has been employed, where Ω_i is the sum of the areas of the surface triangles adjacent to site i. The form of $\beta \tilde{E}_b^{Lap}$ follows from equation (62) by substituting in $\sigma_{ij}/l_{ij} = 1/\sqrt{3}$, the result for equilateral triangles, and noting that $\sum_i \sigma_i = \sum_i \Omega_i/3$.

3.1.4. Simulation methods. The total energy of a network configuration, βE, is give by the sum of the nearest-neighbour, βE_{nn}, and bending, βE_b, energies. A number of Monte Carlo, molecular dynamics, and Langevin methods have been used to determine the thermodynamic behaviour of tethered networks.

Monte Carlo methods are the simplest. A Monte Carlo step consists of an attempt to update the position of each vertex by a random displacement in the cube $[-s, s]^3$. Updates are accepted with a probability equal to $\min[1, \exp(-\delta H_{o,n})]$, where

$$\delta H_{o,n} = \beta E_{old} - \beta E_{new}. \tag{64}$$

s is chosen so that approximately 50% of the attempts are accepted. If there is no explicit bending energy, and hence equations (52) and (56) are the only interaction potentials, all moves are accepted which do not violate the hard-sphere or maximum-tether-length restrictions.

A wide variety of molecular dynamics procedures have also been used to study polymerized networks. Simulations have been performed in the microcanonical ensemble (Abraham *et al* 1989, Abraham and Nelson 1990b), constant-temperature ensemble—using both constraint and Nosé thermostating (Zhang *et al* 1996) as well as heat-bath algorithms (Grest and Murat 1990, Grest 1991, Petsche and Grest 1993, Zhang *et al* 1993)—as well as the (T, σ)-ensemble (Zhang *et al* 1996), where σ is the lateral tension. Since molecular dynamics methods are more efficient when softer potentials are employed, the nearest-neighbour potential is generally taken to be a harmonic or a finitely extensible non-linear elastic potential, while a purely repulsive, shifted and truncated Lennard-Jones potential is used to ensure self-avoidance. A closely related method—the Fourier-accelerated Langevin algorithm—has also been used to study the crumpling transition of self-intersecting networks with an explicit bending rigidity (Harnish and Wheater 1991, Wheater and Stephenson 1993, Wheater 1996). A Monte Carlo renormalization group procedure in momentum space has been employed in conjunction with this approach (Espriu and Travesset 1995, 1996).

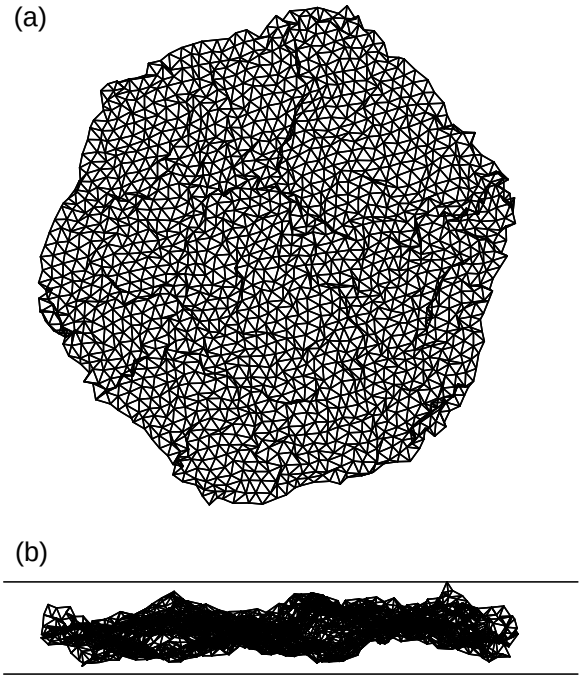

Figure 3. A typical configuration of a polymerized membrane (containing 1801 vertices with tether length $\ell_0 = 1.6\sigma_0$) confined between two parallel walls of separation $9\sigma_0$. Projections (a) onto the wall and (b) parallel to the wall are shown. From Gompper and Kroll (1991a).

3.2. Simulation results

3.2.1. Simulations of the flat phase. MC and MD simulations have shown that polymerized membranes are in a flat phase for sufficiently large bending rigidity. Several methods, such as the analysis of the moments-of-inertia tensor (Boal *et al* 1989), the anisotropic scattering intensity (Abraham and Nelson 1990a), and the pressure exerted on two confining walls (Gompper and Kroll 1991a, b), have been employed to determine the exponents η or ζ which characterize the out-of-plane fluctuations. A typical configuration of a polymerized membrane between two walls is shown in figure 3. Most of these simulations were performed using free-edge boundary conditions. The most precise values of the exponents, however, have been obtained from simulations of vesicles (Zhang *et al* 1993, Petsche and Grest 1993) and tensionless membranes with periodic boundary conditions (Zhang *et al* 1996). In the first case, one finds $\eta = 0.81 \pm 0.03$, or $\zeta = 0.60$ (Zhang *et al* 1993), and $\zeta = 0.58 \pm 0.02$ (Petsche and Grest 1993), while in the second, $\zeta = 0.59 \pm 0.02$ (Zhang *et al* 1996). These values are in good agreement with the theoretical result of Le Doussal and Radzihovsky (1992) quoted above. This settles a debate concerning the possible absence of renormalization of the in-plane elastic constants (Lipowsky and Giradet 1990, Abraham 1991).

For $d = 3$, a negative value of the Poisson ratio has been confirmed in simulations (Zhang *et al* 1996, Falcioni *et al* 1997). Whereas the value obtained using periodic boundary conditions, $\sigma_p = -0.15 \pm 0.01$ (Zhang *et al* 1996), is about a factor two smaller than the theoretical expectation quoted above, a simulation with free-edge boundary conditions yielded $\sigma_p \approx -0.32$ (Falcioni *et al* 1997). The value $\sigma_P = -0.34$ was measured

in Monte Carlo simulations of tethered networks with free-edge boundary conditions for $d = 4$ (Barsky and Plischke 1994).

3.2.2. Crumpling and buckling transitions of phantom membranes. In the absence of self-avoiding restrictions, a crumpling transition is observed with decreasing bending rigidity (Kantor and Nelson 1987a, b). The crumpled phase is characterized by an isotropic scattering intensity and a fractal dimension $d_f = \infty$ (Kantor *et al* 1986, 1987). The most detailed studies of the crumpling transition have been performed using Gaussian spring models. While there is some evidence that the critical behaviour at the crumpling transition might depend on whether expressions (57) or (63) are used for the discretized bending energy (Baig *et al* 1989b, Harnish and Wheater 1991), more recent studies (Baig *et al* 1994) have shown that this is not the case. Baig *et al* (1994) have also shown that the critical behaviour is the same for various surface triangulations and choices of the elastic nearest-neighbour potential. In particular, while models with an elastic energy proportional to the sum of the areas of the elementary triangles are pathological due to the proliferation of spikes for zero bending rigidity (see section 3.1.1), the behaviour at the crumpling transition is the same.

Simulation results in $d = 3$ dimensions (Kantor and Nelson 1987a, Kantor *et al* 1987, Ambjørn *et al* 1989, Renken and Kogut 1990, Harnish and Wheater 1991, Wheater and Stephenson 1993, Baig *et al* 1994, Espriu and Travesset 1996, Wheater 1996, Bowick *et al* 1996) are consistent with a second-order crumpling transition. The most accurate values for the critical exponents were obtained in the three most recent papers. A detailed study of networks containing up to 64^2 nodes with periodic boundary conditions (Wheater 1996) reported the following values for the correlation length exponent $\bar{\nu}$ (not to be confused with the size exponent defined in equation (5)) and the thermal exponent α: a direct measurement of the correlation length exponent from an analysis of the tangent–tangent correlation function yielded the result $\bar{\nu} = 0.71 \pm 0.05$, while a finite-size scaling analysis of the peak in the specific heat, assuming hyperscaling, gave $\bar{\nu} = 0.73 \pm 0.06$. These results imply $\alpha = 0.58 \pm 0.10$. A finite-size scaling analysis of the peak in the specific heat in a study of networks with free-edge boundary conditions containing up to 128^2 nodes (Bowick *et al* 1996) yielded the result $\alpha = 0.40 \pm 0.10$. Bowick *et al* (1996) also found $\eta_c = 0.71 \pm 0.05$ (which corresponds to $d_f \approx 3.1$ (see equation (30))) from an analysis of the decay of the normal–normal correlation function, in reasonable agreement with the theoretical predictions discussed in section 2.1.7. A Monte Carlo renormalization group analysis of data obtained using a Fourier-accelerated Langevin algorithm yielded the result $\eta_c = 0.85 \pm 0.15$ (Espriu and Travesset 1996).

The Gaussian spring model with bending energy (57) has also been studied using Monte Carlo methods in $d = 2$ dimensions (Renken and Kogut 1991a). A finite-size scaling analysis of the data for the specific heat suggests that the crumpling transition is first order in this case. This result is consistent with that obtained for the folding transition of the regular triangular lattice in the presence of a bending rigidity (Di Francesco and Guitter 1994a) (see section 7.2).

The scaling behaviour at the buckling transition has been studied using Monte Carlo methods by Guitter *et al* (1990).

3.2.3. The effect of self-avoidance. The simplest model of tethered self-avoiding membranes is a triangular network of purely repulsive spheres of diameter σ_0. Self-intersection is prohibited if the potentials are chosen so that the spheres cannot penetrate

(a)

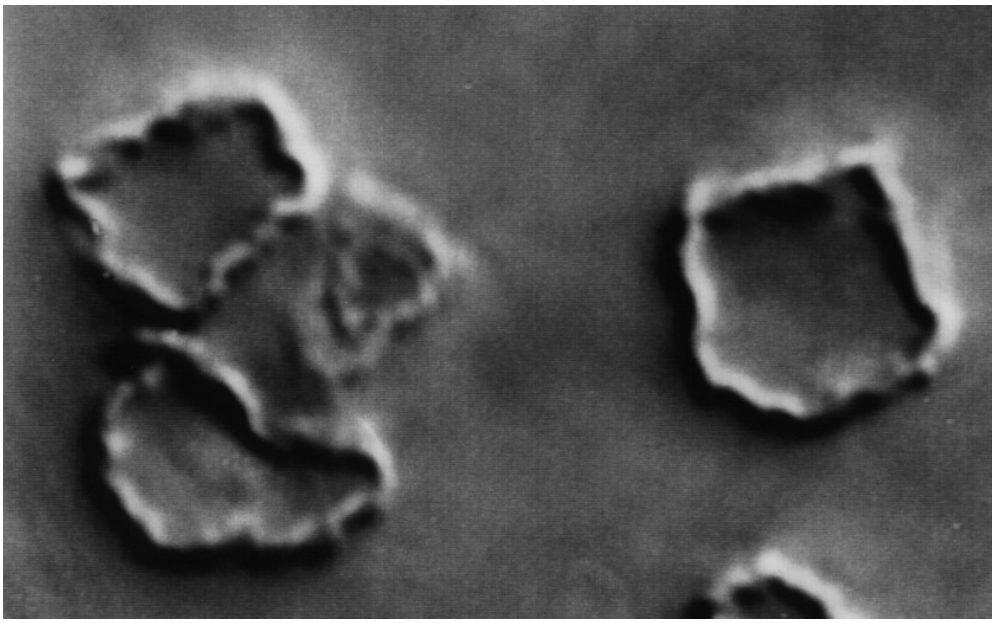

(b)

Figure 4. (a) Cross sections of typical configurations of vesicles containing $N = 16\,002$ monomers with $n = 8$ (Petsche and Grest 1993). (b) Video-enhanced differential interference contrast microscopy images of isolated red-blood-cell cytoskeletons at 25 mM salt concentration. The mean diameter of the cytoskeletons is 5.3 ± 0.4 μm (photograph courtesy of Ch Schmidt). Note the similarity between the shapes of the experimental and simulated networks.

an elementary triangle of the network. It was first shown by Abraham *et al* (1989), and later confirmed by others (Ho and Baumgärtner 1989, Abraham and Nelson 1990a, b, Grest 1991, Gompper and Kroll 1991a, b) that self-avoidance completely suppresses the crumpling transition, so self-avoiding membranes are in the flat phase even without an explicit bending rigidity.

It has been argued by Abraham and Nelson (1990b) that a bending rigidity is generated for entropic reasons by excluded-volume interactions, even if there is no explicit bending energy. In fact, such a term is generated already upon the introduction of next-nearest-

neighbour interactions, and, for the standard tether-and-bead model discussed in the previous paragraph, this effective rigidity is larger than that required to produce the flat phase in phantom membranes. This effective rigidity is proportional to the temperature, so changing the temperature does not modify the strength of this effect. This argument leaves open the possibility that more flexible surfaces might crumple. Subsequently, simulations have been performed on tethered networks in which linear chains of n monomers are connected to form either a hexagonal lattice (Abraham 1992, Abraham and Goulian 1992) or a triangular lattice (Petsche and Grest 1993). The largest simulations have been performed on networks consisting of $N = 29\,420$ monomers for open membranes (Abraham 1992, Abraham and Goulian 1992) and $N = 25\,002$ for vesicles (Petsche and Grest 1993), both for $n = 8$. Three cross sectional views of typical configurations of vesicles containing $N = 16\,002$ monomers with $n = 8$, are shown in figure 4. Video-enhanced differential contrast microscopy images of isolated red-blood-cell cytoskeletons at high salt concentration (Schmidt *et al* 1993) are also shown. Note the similarity between the conformations of the red-blood-cell cytoskeletons and the simulated network.

There have also been several studies of models in which the effective size of the particles at the vertices, σ_0, is decreased (Abraham *et al* 1989, Boal *et al* 1989, Kantor and Kremer 1993, Barsky and Plischke 1994), or the triangular network is site (Grest and Murat 1990) or bond (Plischke and Fourcade 1991) diluted. Self-avoidance can also be guaranteed by requiring that the elementary surface triangles of the network do not self-intersect (Baumgärtner 1991, Baumgärtner and Renz 1992, Kroll and Gompper 1993). This results in a very flexible surface which can fold on itself without any cost in energy. The resulting surfaces are therefore much rougher than those constructed with hard-core repulsion for small n, and are, in fact, very similar to the tethered-chain models in the limit of large n. In all of these cases—with the exception of Baumgärtner (1991) and Baumgärtner and Renz (1992), where a crumpled phase has been claimed—however, the membranes were found to remain flat, even though the local bending rigidity is quite low. This suggests that the interactions inducing the rigidity, whatever they are, are relevant under renormalization.

The spherically averaged structure function $S(q, L)$ is generally what is measured in experimental studies of tethered membranes. However, special care must be exercised in the interpretation of these measurements, since it is often difficult to discern the difference between the directionally averaged scattering function of a flat, rough membrane and a truly crumpled membrane. Indeed, in the first simulation studies of open tethered networks (Kantor *et al* 1986, 1987), the results for the structure function were interpreted in terms of a crumpled phase characterized by a scaling exponent $\nu = 0.83 \pm 0.03$. However, as discussed in section 2.1.8, the directionally averaged structure factor should scale as $q^{-3+\zeta}$ in the flat phase for a wide range of q if the amplitude of the undulation modes is larger than that of the phonon modes (Goulian *et al* 1992). Using $\zeta = 0.6$, this is roughly consistent with the behaviour observed by Kantor *et al* (1986, 1987). The results of subsequent, more detailed studies of very flexible open networks (Abraham and Goulian 1992, Kroll and Gompper 1993) are consistent with this interpretation. Abraham and Goulian (1992) have found that the isotropically averaged structure factor scales as $q^{-2.35}$ for a wide range of q, consistent with an exponent $\zeta = 0.65$. Simulations of impenetrable plaquette models (Kroll and Gompper 1993) yield a structure factor that scales as $q^{-2.7}$ for intermediate wavevectors, which appears to lie between the two regimes $1/q^{-3+\zeta}$ and $q^{2-4/\zeta}$ predicted by Goulian *et al* (1992) and discussed in section 2.1.8. Recent x-ray and light scattering experiments (Schmidt *et al* 1993) on isolated red-blood-cell cytoskeletons at high salt concentrations measured a directionally averaged scattering function in which a q^{-2}-regime was followed by a $q^{-2.35}$-regime for larger q, again consistent with the behaviour expected for a flat

membrane. The result for intermediate wavevectors is consistent with that obtained in simulation studies of tethered vesicles (Zhang *et al* 1993, Petsche and Grest 1993).

Polymerized membranes have also been studied for spatial dimensions larger than three. As discussed in section 2.1.5, self-avoidance should become less important in this case, and the network is more likely to be crumpled. Indeed, a crumpled phase is found for dimensions $d \geqslant 5$ (Grest 1991, Barsky and Plischke 1994). This finding is in agreement with analyses of the generalized Edwards model with two-body interactions using a Gaussian variational approximation (Goulian 1991) and an expansion in a large embedding space d (Le Doussal 1992). It was found that the flat phase is stable for $d = 3$ and that tethered membranes are crumpled for $d > 4$, with the scaling exponent ν approaching one (with logarithmic corrections) for $d \to 4$. For $d > 4$, the results for the fractal dimension d_f are much closer to the simulation results than the Flory prediction (8). Guitter and Palmeri (1992) used a variational approach for large d, and found that for $d = 3$, tethered membranes lie exactly on the boundary of the stable flat phase. Le Doussal and Radzihovsky (1992) have used the self-consistent screening approximation to obtain the estimate that the upper critical dimension is $d_{uc} \approx 4.98$.

An alternative interpretation of the simulation results is suggested by the prediction of Flory theory that four-body interactions are relevant below four dimensions and three-body interactions are relevant below six dimensions (see section 2.1.5). Thus, if three-body interactions are sufficient to generate an effective rigidity, Flory theory predicts that tethered networks should crumple above six dimensions. While the critical dimensions suggested by Flory theory should not be taken too seriously, this argument may provide some insight into the origin of the observation that self-avoiding tethered surfaces are crumpled only for $d \geqslant 5$.

In order to gain further insight into the influence of excluded-volume interactions on determining whether a network is crumpled or flat, it would be interesting to be able to vary not only the spatial dimension d, but also the internal dimension D of the network. While this cannot be done for homogeneous networks in simulations, it was argued in section 2.1.6 that polymeric fractals are a useful generalization to consider (Grest 1991). These networks are characterized by a spectral dimension, d_s, which describes the intrinsic connectivity of the network, and—at least in the Flory approximation—plays the same role as D. Levinson (1991) found that the fractal dimension of self-intersecting Sierpinski gaskets (which have a spectral dimension $d_s = 2 \ln 3 / \ln 5 \approx 1.365$ (Gefen *et al* 1981)) embedded in dimension d where $3 \leqslant d \leqslant 8$ is in good agreement with the Flory prediction (16). Similarly, Grest and Murat (1990) have confirmed the Flory prediction $d_{f_0} = 4$ for percolation clusters at the percolation threshold.

Self-avoidance is a relevant perturbation for spatial dimension $d < d_{uc}$ where d_{uc} is given by equations (12) and (17) for homogeneous networks and polymeric fractals, respectively. There are a number of self-avoiding networks where the Flory estimate for d_f, equation (19), accurately describes the scaling behaviour for $d < d_{uc}$. These include linear polymers in two and three dimensions, percolation clusters at the percolation threshold (for which $d_s \simeq 4/3$ in all dimensions (Alexander 1982)) in two and three dimensions (Grest and Murat 1990), and Sierpinski gaskets for $3 \leqslant d \leqslant d_{uc} \approx 8.6$ (Levinson 1991). In all these cases, any deviation from Flory theory is very small.

Three examples where Flory theory is *qualitatively* wrong are Sierpinski gaskets for $d = 2$ (Duering and Kantor 1989) and two-dimensional tethered networks in three and four dimensions. In contrast to the systems discussed in the last paragraph, in all of these cases higher-order n-body interactions are relevant. A phase diagram for polymeric fractals (Grest 1991, Levinson 1991) which shows where the crumpled and flat phases are stable in the

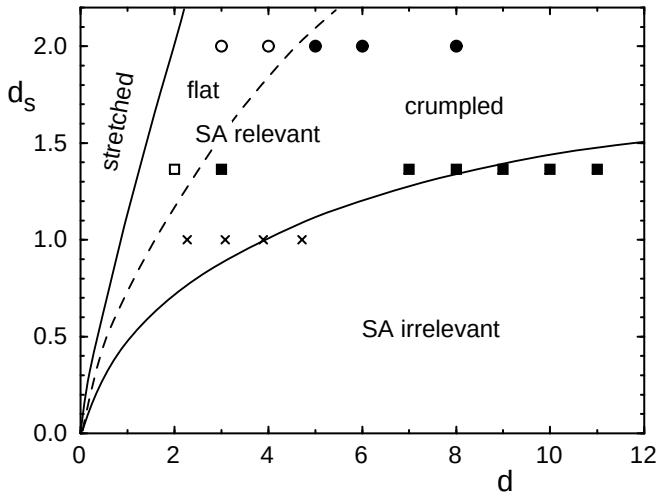

Figure 5. The phase diagram for polymeric fractals. The regions of stability of the crumpled and flat phases are indicated. The crosses represent data for linear polymers, $d_s = 1$, the squares are for Sierpinski gaskets (Duering and Kantor 1989, Levinson 1991), and the circles are for two-dimensional tethered membranes (Grest 1991, Barsky and Plischke 1994). The open symbols are in the flat phase and the closed symbols and crosses are in the crumpled phase. The dashed line separates the flat and crumpled phases; self-avoidance (SA) is relevant above the solid line, and irrelevant below it. Redrawn from Grest (1991).

(d_s, d) plane is presented in figure 5. It would be interesting to have results for systems with $d_s > 2$, such as gels embedded in $d > 3$ dimensions, in order to describe in more detail the phase boundary between the flat and crumpled regimes. Similarly, further results for systems with d_s in the range 4/3 to 2 might help to provide an understanding of why the Flory estimate for d_f is so good for values of d_s near one, but fails for $d_s = 2$ (Grest 1991, Grest and Murat 1995).

3.2.4. Attractive interactions. Another possible way to drive a polymerized membrane into the crumpled phase is to include an attractive interaction between all vertices—in addition to the hard-sphere repulsion. Two cases which have been studied so far are square-well and van der Waals interactions. In the first case, a crumpled phase with fractal dimension $d_f = 2.5$ was found over a very narrow range of temperatures (Liu and Plischke 1992). In the second case, a sequence of folding transitions, but no crumpling, was observed (Abraham and Kardar 1991, Münkel and Heermann 1995). The low-temperature phase in both cases is a collapsed state of fractal dimension $d_f = 3$, in agreement with the Flory result discussed in section 2.1.3.

Grest and Petsche (1994) have combined weak self-avoidance (short polymer chains of length n between vertices) and attractive (van der Waals) interactions to search for a crumpled phase of tethered vesicles. For $n = 4$, a first-order transition between a high-temperature flat phase and a low-temperature collapsed phase was found. However, for $n = 8$, the transition seems to be second order, with a crumpled phase of fractal dimension $d_f \simeq 2.4$ at the transition point.

3.2.5. Forced crumpling of elastic sheets. The most obvious way to obtain a crumpled state of an elastic sheet is to apply an external force and to crush the sheet into a small confining

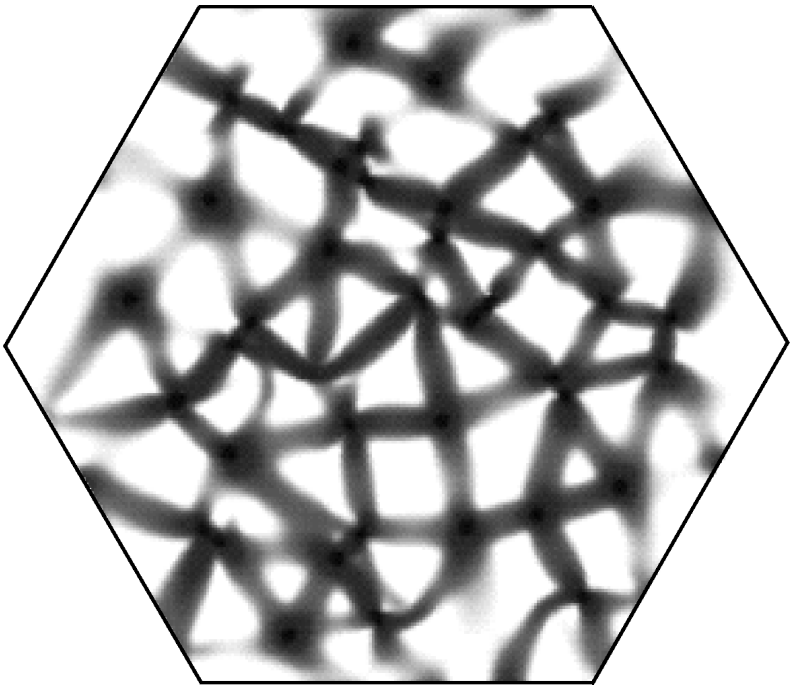

Figure 6. The curvature energy distribution in a hexagonal sheet of diameter $L = 160a_0$ (where a_0 is the equilibrium spring length) which has been crushed into a sphere of radius $R_0 \simeq L/6$. Darker regions have higher energy density. From Kramer and Witten (1997).

volume. This was already done several years ago in a 'desktop experiment' (Kantor *et al* 1987) in an attempt to determine the exponent ν of the radius of gyration of thermally crumpled membranes. Very recently, Kramer and Witten (1997) studied this question much more carefully. They use a triangular network of springs with bending rigidity to model the elastic sheet. This network is then compressed by slowly decreasing the radius of a confining sphere. They show that after compression, most of the elastic energy is contained in point-like vertices and in a network of 'stretching ridges'; see figure 6. The scaling behaviour of ridges of length R was determined in earlier studies of the asymptotic shape of large fullerene balls—flat-sided icosahedra with smooth edges (Witten and Li 1993, Lobkovsky *et al* 1995, Zhang *et al* 1995)—and other regular polyhedra (Lobkovsky *et al* 1995, Lobkovsky 1996), where it was shown that the width of a stretching ridge scales as $R^{2/3}$, and its energy as $R^{1/3}$. For phantom networks, the length of a ridge in the confining sphere is proportional to the sphere radius, R_0, so the number of ridges in a sheet of internal dimension L is approximately $(L/R_0)^2$. The total energy of the (phantom) crushed sheet should therefore scale as $R_0^{-5/3}$; this result is supported by the simulation data (Kramer and Witten 1997).

The buckling of (isolated) ridges under compression by an external force which is applied either parallel or perpendicular to the ridge axis has also been investigated (Lobkovsky and Witten 1997).

3.2.6. Membranes with quenched internal disorder. Three types of quenched disorder in polymerized membranes have been studied during the last few years: size impurities (Kantor 1992, Mori 1996b), random polymerization (Nelson and Radzihovsky 1991, Radzihovsky

and Nelson 1991, Morse *et al* 1992b), and random spontaneous curvature (Morse and Lubensky 1992, Morse *et al* 1992a). Theoretical analyses—based on renormalization group theory—lead to the conclusion that for any finite temperature, $T > 0$, *weak* short-range disorder is irrelevant (Nelson and Radzihovsky 1991, Radzihovsky and Nelson 1991). However, at $T = 0$, the situation is found to be more complicated. In phantom membranes, *size impurities*—which correspond to randomness in the local preferred metric—lead to a softening of the bending rigidity and a destabilization of the flat phase in favour of a crumpled glass phase (Nelson and Radzihovsky 1991, Radzihovsky and Nelson 1991, Radzihovsky and Le Doussal 1992); Monte Carlo simulations (Kantor 1992) confirm this result. For *random spontaneous curvature*, on the other hand, the bending rigidity is predicted to stiffen at long wavelengths, resulting in a new flat phase with anomalous statistical and elastic properties (Morse and Lubensky 1992, Morse *et al* 1992a, b). Numerical simulations (Morse *et al* 1992a, b) are again in agreement with these predictions.

The possibility of a crumpled phase even for $T > 0$ for *strong* short-range disorder has been discussed by Radzihovsky and Le Doussal (1992), Bensimon *et al* (1992), and Mori and Wadati (1994). Mean-field analyses of models with random internal stresses (Radzihovsky and Le Doussal 1992) and random spontaneous curvature (Bensimon *et al* 1992) both predict that the flat phase becomes unstable towards a crumpled glass phase analogous to a spin glass for $T > 0$. Mori and Wadati (1994) used a Gaussian variational method and concluded that for strong disorder in the preferred metric, self-avoiding membranes with a small bending rigidity are in a crumpled phase characterized by a radius-of-gyration exponent $\nu = 6/7$. This result is supported by Monte Carlo simulations of weakly self-avoiding tethered membranes with site impurities (Mori 1996b) and tethered membranes created by random polymerization of fluid films (Mori 1996a).

Le Doussal and Radzihovsky (1993) have used the self-consistent screening approximation to show that, depending on the range of the disorder, several new glassy phases are stable at $T > 0$ in polymerized membranes with weak *long-range* disorder in the preferred metric and/or the extrinsic curvature.

4. Models of fluid membranes

4.1. Randomly triangulated surfaces

For simulation studies of fluid membranes, the network model introduced in section 2.2 has to be modified to allow for the diffusion of vertices in the membrane. This is done by making the connectivity of the network a dynamic variable. The simplest way to do so is to cut and reattached tethers between the four beads of two neighbouring triangles (Kazakov *et al* 1985, Boulatov *et al* 1986, Billoire and David 1986, Ho and Baumgärtner 1990, Kroll and Gompper 1992a, Boal and Rao 1992a).

An interesting extension of the above algorithm called ‘baby universe surgery’ has recently been suggested (Ambjørn *et al* 1994). The method is useful for the simulations of closed surfaces when there is an appreciable probability for minimal necks, i.e. loops consisting of three bonds that divide the surface into two parts. Such minimal necks are, for example, common in the branched polymer phase, where there is a proliferation of long, thin arms. The new Monte Carlo move consists of cutting the surface in two at the neck and gluing the two surfaces back together in a way chosen at random. This procedure is clearly more efficient for phantom surfaces; however, it should also be useful in simulations of self-avoiding random surfaces for small bending rigidities. Baby universe surgery has

been used in a number of simulation studies of two-dimensional quantum gravity, both with and without matter fields. See Ambjørn *et al* (1995a, c) for references.

4.2. Renormalization of the bending rigidity

All current attempts to determine the renormalization of the bending rigidity from Monte Carlo simulations are based on the scaling behaviour of the average volume $\langle V \rangle$ of fluctuating vesicles of (approximately) constant area A. The analogy with the behaviour of the enclosed area of ring polymers in two spatial dimensions (Camacho *et al* 1991) suggests the scaling form

$$\langle V \rangle A^{-3/2} = \Theta_V(\sqrt{A}/\xi_p) \tag{65}$$

where $\xi_p = a \exp[(4\pi\kappa)/\alpha_\kappa]$ is the persistence length. Data obtained from Monte Carlo simulations are indeed consistent with this scaling *ansatz* for $\alpha_\kappa = 3.3 \pm 0.5$ (Gompper and Kroll 1995b, Ipsen and Jeppesen 1995). However, the analytic result (42) for $\langle V \rangle$ in the limit of large κ is *inconsistent* with the scaling *ansatz* (65). Therefore, corrections to scaling have to be taken into account (Gompper and Kroll 1996). To gain some insight into the behaviour for moderate κ, the effect of the scale dependence of the bending rigidity has been incorporated in equation (40) by replacing κ by $\kappa_R(\ell)$; compare equation (43). This implies (Gompper and Kroll 1996)

$$\langle V \rangle / V_0 - 1 + \frac{3}{2\alpha_\kappa} \ln(4\pi\kappa/\alpha_\kappa) = \Theta_V(\sqrt{A}/\xi_p). \tag{66}$$

The Monte Carlo data scale about as well with the new scaling form—again with $\alpha_\kappa \simeq 3$—as they do with equation (65).

4.3. The phase diagram of fluid vesicles

The phase diagram of self-avoiding fluid vesicles as a function of the bending rigidity κ and a pressure increment Δp between the vesicle's interior and exterior has been determined from Monte Carlo simulations (Gompper and Kroll 1994, 1995b). For very small bending rigidities and small or negative Δp, vesicles are found to collapse into a branched-polymer-like phase (Kroll and Gompper 1992a, b, Boal and Rao 1992a, Baillie and Johnston 1992), which is characterized by the scaling laws

$$\langle V \rangle \sim N \tag{67}$$

$$\langle R_g^2 \rangle \sim N^{\nu_{bp}} \tag{68}$$

for the average volume and radius of gyration, with $\nu_{bp} = 1$. A typical configuration is shown in figure 7(a). A more detailed characterization can be obtained by studying random walks on these surfaces; their behaviour determines the spectral dimension d_s. The mean square displacement after t steps of a random walk on a surface of N monomers is expected to scale as (Gefen *et al* 1983, Komura and Baumgärtner 1990)

$$\langle [\boldsymbol{r}(t) - \boldsymbol{r}(0)]^2 \rangle = N^{\nu} f(t/N^{2/d_s}) \tag{69}$$

where the scaling function $f(x) \sim x^{d_s/d_f}$ for $x \ll 1$ and $f(x) =$ constant for $x \gg 1$. Simulation data indeed collapse onto a universal scaling function for $d_s = 1.25 \pm 0.04$ (Kroll and Gompper 1992b), which is in excellent agreement with the best estimates for branched polymers (Havlin *et al* 1984). Earlier claims of a crumpled phase of fluid membranes characterized by $\nu_{bp} \simeq 0.8$ (Baumgärtner and Ho 1990, Ho and Baumgärtner 1990) and $d_s = 2$ (Komura and Baumgärtner 1990) have not been confirmed.

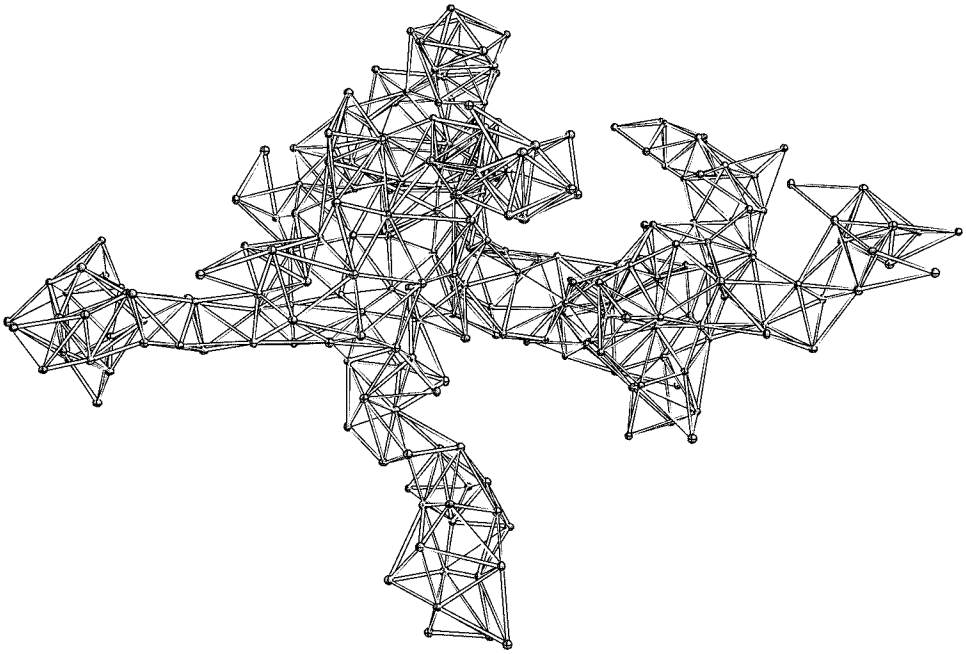

(a)

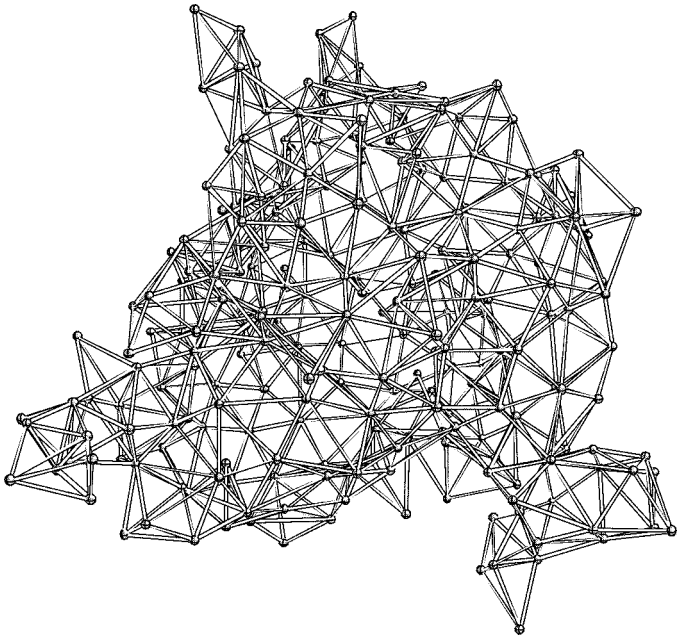

(b)

Figure 7. Typical configurations of fluid vesicles (containing 247 vertices with tether length $\ell_0 = 1.67\sigma_0$) in the entropy-dominated regime. (a) The branched-polymer-like configuration at bending rigidity $\kappa \ll 1$ and small pressure increment Δp. (b) The inflated configuration at bending rigidity $\kappa \ll 1$ and sufficiently large and positive Δp. (c) The branched-polymer-like configuration at bending rigidity $\kappa \simeq 1.4$ and negative Δp. From Gompper and Kroll (1995b).

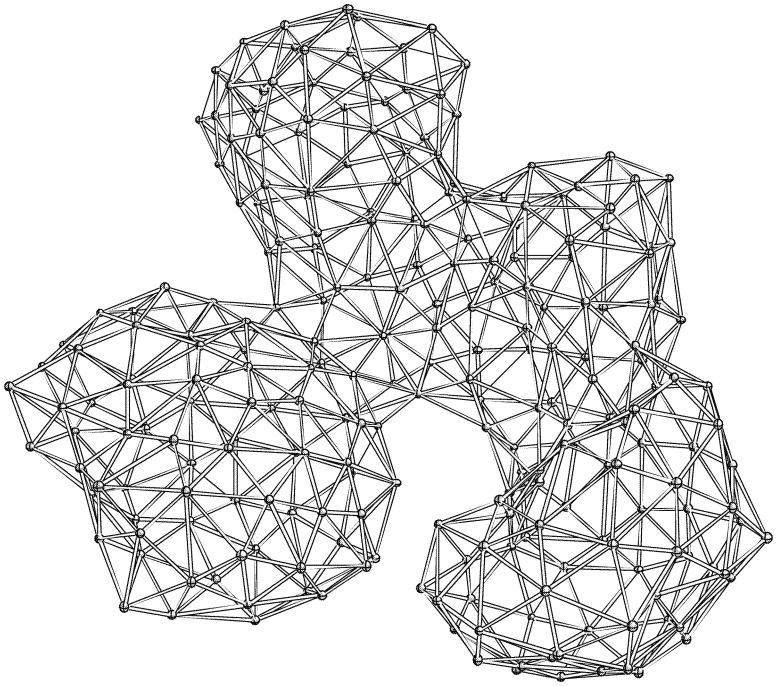

(c)

Figure 7. (Continued)

With increasing pressure increment Δp, a first-order transition to an 'inflated' phase occurs (Gompper and Kroll 1992b, c, Dammann *et al* 1994). The transition pressure p^* scales with the membrane size N as

$$p^* \sim N^{-\zeta_+} \tag{70}$$

with an exponent in the range $\zeta_+ = 0.5$ (Gompper and Kroll 1992b) to $\zeta_+ = 0.65 \pm 0.05$ (Gompper and Kroll 1994) and $\zeta_+ = 0.69 \pm 0.01$ (Dammann *et al* 1994). The differences in the values of ζ_+ are mainly due to the different data analyses. The value of $\zeta_+ = 0.5$ is obtained when finite-size corrections are taken into account by replacing N in equation (70) by $(N - N_0)$, with $N_0 = 40$. The presently available range of system sizes does not allow a clear distinction between these two values of ζ_+.

Just above the transition, the vesicle is roughly spherical, but its surface is still very rough; see figure 7(b). With further increasing pressure, it approaches the shape of a perfect sphere. This approach can again be described by a scaling law. In analogy with the analysis of the shape of inflated ring polymers (Maggs *et al* 1990), the average volume of the vesicle is predicted to scale as (Gompper and Kroll 1992b, c)

$$\langle V \rangle = V_0 p^{3\omega_+} N^{3\nu_+} \tag{71}$$

where

$$\omega_+ = \frac{1-\nu}{3\nu - 1} \qquad \nu_+ = \frac{\nu}{3\nu - 1}. \tag{72}$$

Monte Carlo simulations confirm this scaling form with an exponent $\nu = 0.787 \pm 0.020$ (Gompper and Kroll 1992b, c). A similar scaling analysis applies to the moments of inertia

λ_i, which determine the asphericity of vesicle shapes. The same arguments as those that lead to equation (71) indicate that (Gompper and Kroll 1992c, Baumgärtner 1993b)

$$\frac{3\langle\lambda_i\rangle}{\langle\lambda_1+\lambda_2+\lambda_3\rangle}-1=\Gamma_i(\langle V\rangle N^{-3\nu/2}). \tag{73}$$

The scaling functions $\Gamma_i(x)$ are expected to decay asymptotically as $\Gamma_i(x)\sim x^{-1/(3-3\nu)}$ as the vesicle shape becomes spherical. Monte Carlo data for the smallest and largest eigenvalues nicely follow this power-law behaviour, with an exponent ν which is very close to the value quoted above (Gompper and Kroll 1992c).

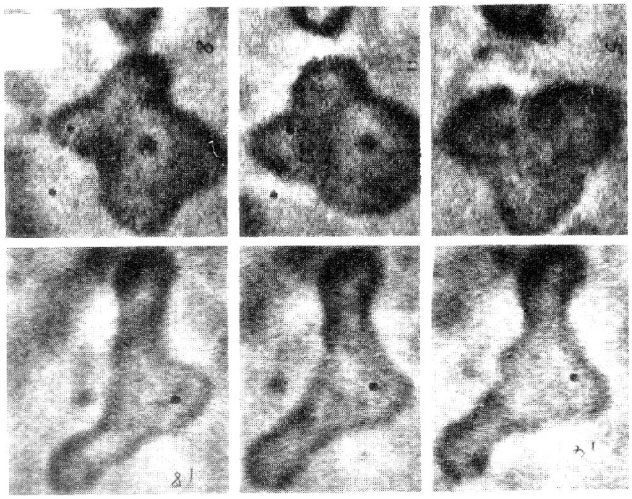

Figure 8. Transient shapes of vesicles of DMPC containing 2 mol% of the bipolar lipid denoted as bola lipid. The images were recorded from top left to bottom right; the time interval between two images is about 10 s. From Duwe *et al* (1990).

The entropy-dominated phases are stable for $\kappa\lesssim 2$. A typical configuration for bending rigidity $\kappa\simeq 1.4$ is shown in figure 7(c). Such vesicles shapes have been observed experimentally by Duwe *et al* (1990); see figure 8. For larger bending rigidities, the curvature energy dominates, and prolates, discocytes and stomatocytes are the shapes of minimal free energy (compare Seifert *et al* (1991), Seifert (1997)). The full phase diagram obtained from simulations of a network of $N=247$ vertices is shown in figure 9.

It is interesting to note that the branched polymer behaviour for small bending rigidity remains unchanged when the genus of the vesicle is allowed to fluctuate (Jeppesen and Ipsen 1993).

4.4. Phase behaviour of phantom membranes as a function of the bending rigidity

The behaviour of phantom fluid membranes is quite different from that of self-avoiding surfaces for very small bending rigidities. Since phantom polymerized membranes are crumpled, with a radius of gyration which increases only logarithmically with system size (compare sections 2.1.5 and 3.1.1), it is natural to expect similar behaviour for phantom fluid membranes; this has indeed been found in simulations (Ambjørn *et al* 1985, Baillie *et al* 1990). However, most simulation results suggest a large but *finite* fractal dimension (Boulatov *et al* 1986, Billoire and David 1986, Münkel and Heermann 1992). In fact,

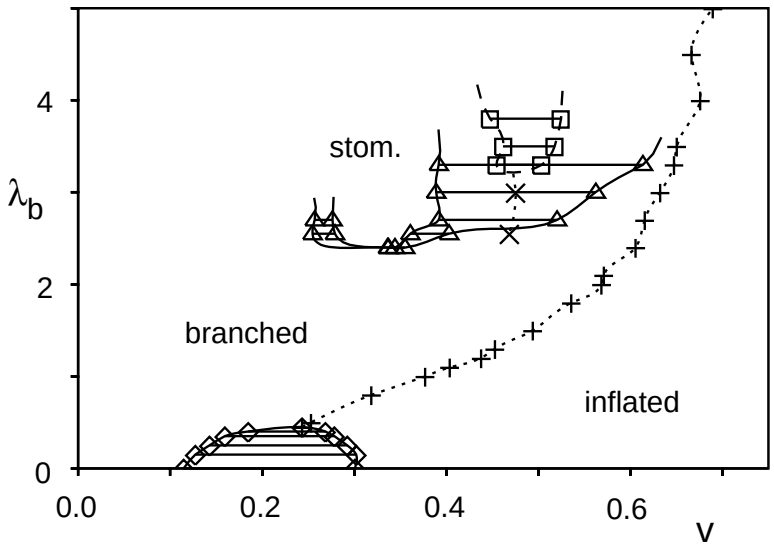

Figure 9. The phase diagram of fluid vesicles in the pressure ensemble, as a function of the reduced volume $v = \langle V \rangle / V_0$ and the bending rigidity λ_b, for $N = 247$. Compressibility maxima are shown by a dotted line, the dumb-bell-to-metastable discocyte transition by a dashed line. From Gompper and Kroll (1995b).

there are strong indications that the scaling properties depend on short-distance properties of the triangulation and appear to be *non-universal* (Boulatov *et al* 1986, Billoire and David 1986). It is tempting to speculate that the finite fractal dimension is due to the contribution of branched-polymer-like configurations.

A question of particular interest is the phase behaviour as a function of the bending rigidity (for zero pressure increment). There have been several papers (Catterall 1989, Baillie *et al* 1990, 1991, Renken and Kogut 1991b, Bowick *et al* 1993, Anagnostopoulos *et al* 1993, Ambjørn *et al* 1993, 1995b) reporting a phase transition between a low-bending-rigidity 'crumpled' phase and a high-bending-rigidity 'smooth' phase for the Gaussian spring model of non-self-avoiding surfaces. The existence of such a transition was concluded from a peak in the specific heat, which has been determined to occur at $\lambda_b = 1.425 \pm 0.010$ (Anagnostopoulos *et al* 1993) and $\lambda_b = 1.50 \pm 0.03$ (Ambjørn *et al* 1993) for the discretization (57) of the bending rigidity, and for $\tau \simeq 0.75$ (Baillie *et al* 1990) for the discretization (63). However, the peak height increases only very slowly with the system size N, and appears to saturate for large N (Anagnostopoulos *et al* 1993, Ambjørn *et al* 1993, Münkel and Heermann 1993). The same behaviour was seen in a tether-and-bead model of self-avoiding surfaces (Kroll and Gompper 1992a).

Several explanations for this peak in the specific heat are possible. First, it could be a second-order transition with a negative specific-heat exponent α. This is the point of view taken by Bowick *et al* (1993), Anagnostopoulos *et al* (1993), and Ambjørn *et al* (1993). Second, it has been argued by Kroll and Gompper (1992a) that the peak is due to a finite-size effect of the persistence length becoming comparable to the system size. In this case, the peak position should decrease logarithmically with N; this has been clearly ruled out by Anagnostopoulos *et al* (1993), who have shown that the peak position approaches a finite limit for large N. Third, it could be a smooth crossover, as it occurs in two-dimensional models of Heisenberg ferromagnetism (Polyakov 1986). The surface normal vectors are

like a spin field, and a crumpled surface is like a Heisenberg paramagnet. The undulations which destroy long-range order in the surface normals are similar to spin waves (Kantor and Nelson 1987a). Indeed, the behaviour of the specific heat of the Heisenberg model—in which the absence of a phase transition can be shown exactly—is very similar to that of the specific heat of the random-surface models (Anagnostopoulos *et al* 1993).

4.5. Vesicle dynamics

The dynamical behaviour of vesicles in external flow fields and the driven transport of vesicles through narrow passages are problems of fundamental interest with potential biological (Lipowsky and Sackmann 1995) and medical applications (Cevc *et al* 1996). Vesicle dynamics has been studied in both elongational (Gompper and Kroll 1993, Kroll and Gompper 1995) and shear (Kraus *et al* 1996) flow fields. In the first case, very-low-bending-rigidity vesicles (in the branched polymer phase) were considered in the free-draining approximation. It was shown that there is no sharp crumple–stretch transition (in analogy to the coil–stretch transition for polymers (de Gennes 1974)); rather, the vesicles were found to slowly elongate with increasing flow rate until they are completely extended into long, thin cylinders.

The behaviour in shear flow has been studied in the opposite limit, that of very large bending rigidity (no thermal fluctuations). Hydrodynamic interactions were included using an Oseen tensor formalism (Kraus *et al* 1996). Whereas discocytes are stable for $v \lesssim 0.75$ in the absence of flow, the stationary shape of the vesicles was found to be an elongated ellipsoid for all reduced volumes $v = V/V_0 > 0.52$, even for very small shear rates $\dot{\gamma}$. The stationary state of a vesicle in the flow field is characterized by both a finite inclination angle θ between the longest axis of the vesicle and the flow direction, and a 'tank-treading' tangential motion of the membrane with rotation frequency ω. It was shown (Kraus *et al* 1996) that the average reduced rotation frequency $\bar{\omega}/\dot{\gamma}$ and the inclination angle decrease with decreasing reduced volume v—with $\bar{\omega}/\dot{\gamma} = 0.5$ and $\theta = \pi/4$ in the spherical limit, in agreement with results for rigid spheres and fluid drops with infinite surface tension (van de Ven 1989). Both quantities were found to be independent of the shear rate within the numerical accuracy.

The driven transport of vesicles through a linear array of narrow pores by the gradient of an applied (electric or gravitational) field has been studied by Monte Carlo simulations (Gompper and Kroll 1995a). In the free-draining approximation, the mobility of the vesicles was found to increase sharply when the strength f of the driving field exceeded a threshold value f^*. For $f > f^*$, the mobility saturates at a value which is essentially independent of the strength of the driving field. The threshold field strength f^* was found to depends on pore radius r_p, vesicle area A, and bending rigidity κ as

$$f^* \sim \kappa^{1+\beta_t} A^{-3/2+\eta_t} r_p^{-2\eta_t} \tag{74}$$

with $\beta_t \simeq 0.2$ and $\eta_t \simeq 2.4$ (Gompper and Kroll 1995a). The strongly non-linear transport properties of vesicles in this geometry can be understood from the balance of bending and potential energies. The potential energy dominates for small and large protrusions Δz of the membrane into the pore, while the bending energy dominates for Δz of order r_p. This leads to a nucleation barrier, the height of which is determined by the field strength. In the zero-temperature limit, the barrier height vanishes at $f = f^*$. In this limit, $\beta_t = 0$ and $\eta_t \simeq 1.55$ have been obtained from an analysis of the shape equations (Gompper and Kroll 1995a).

The dynamics of phase separation and shape deformation in two-component vesicles

has been investigated (Taniguchi 1996) by means of a numerical solution of time-dependent shape equations. The coarsening process of the domain structures was found to be considerably slower (with an effective dynamic exponent $z \simeq 0.1$) than for rigid surfaces (where $z = 1/3$). The phase separation dynamics of a two-component fluid membrane has also been studied using Monte Carlo methods (Kumar and Rao 1996).

4.6. Stacks of fluid membranes and adhesion

The adhesion/unbinding behaviour of membranes at a planar wall and the strength of the inter-membrane entropic repulsion in lamellar phases have been two of the principal questions addressed in the field of membrane physics (Helfrich 1978, Lipowsky and Leibler 1986, Lipowsky and Sackmann 1995, Lipowsky 1995). Monte Carlo simulations of a tethered membrane near a wall have been used to determine the roughness exponent ζ of polymerized membranes (Leibler and Maggs 1989). Simulations of effective solid-on-solid models (in which overhangs are ignored) have been employed to study the unbinding transitions of both single membranes (Lipowsky and Zielinska 1989, Ambjørn *et al* 1996) and of bunches of membranes (Cook-Röder and Lipowsky 1992, Netz and Lipowsky 1993, 1995).

Simulations of solid-on-solid models for stacks of several membranes confined between two hard walls have also been performed in order to determine the universal amplitude c_∞ of the steric interaction between fluctuating membranes (Janke *et al* 1989, Gompper and Kroll 1989). The results are in good agreement with simulation data obtained using similar models for a stack which is confined by a single wall and an external pressure (Netz and Lipowsky 1995). The value, $c_\infty \simeq 0.11$, obtained from these simulations is about a factor two *smaller* than the value obtained theoretically by Helfrich (1978) and confirmed experimentally (Safinya *et al* 1986). It is possible that the discrepancy between experimental and simulation results can be explained by the asymmetry of the ternary system used in the experiments (Netz 1995).

4.7. Fluid membranes with edges

The survival of cells depends critically on the mechanical stability of lipid bilayer membranes against rupture. This stability can be explained by the line tension of the free edge of a bilayer, where the lipid molecules have to adjust to the high local curvature of the monolayer. The (free) energy of a single hole of area A and perimeter length L in a membrane with line tension λ_e and lateral tension σ is given by (Litster 1975)

$$F_{hole} = \lambda_e L - \sigma A. \tag{75}$$

For a circular hole of radius r, one has $A = \pi r^2$ and $L = 2\pi r$. Thus, small holes of radius $r < r_c = \lambda_e/\sigma$ are stable and disappear spontaneously after formation, while large holes of radius $r > r_c$ grow and rupture the membrane.

The picture presented above ignores the entropic contributions from the fluctuations of the hole perimeter. For sufficiently large holes, the entropy should be similar to the entropy of ring polymers, which scales linearly with the polymer length. This leads to a renormalization of the (effective) line tension, $\lambda_{eff} = \lambda_e - b$, in equation (75), where b is a constant of order unity (note that λ_e is measured in units of $k_B T$). The effective line tension can become very small or even negative, so holes can form spontaneously even in membranes without tension (Shillcock and Boal 1996).

Monte Carlo simulations of a tether-and-bead model for fluid membranes with holes confirm this picture (Shillcock and Boal 1996). Furthermore, they show that for tensionless

membranes, large holes appear at a reduced line tension $\lambda_e\sigma_0 \simeq 1.24$ for tether length $\ell_0 = \sqrt{3}$. In this case, holes of *fixed* perimeter length show the same scaling behaviour as self-avoiding random walks. In contrast, holes in membranes under compression scale as branched polymers. In the case of membranes under tension, no simple scaling behaviour has been found.

The simulations have also been used to determine the rupture rate for membranes under tension. The observed dependence of the rupture rate on the line tension follows roughly an exponential Arrhenius law, with a free-energy barrier intermediate between those of circular and self-avoiding holes.

The edge tension is also the reason that membranes form vesicles. It is easy to see that a planar, circular patch of a fluid membrane is energetically unfavourable compared to a spherical vesicle when the patch radius exceeds $r^* = 4(2\kappa + \bar{\kappa})/\lambda_e$ (Helfrich 1974). The effect of thermal fluctuations has been studied by Monte Carlo simulations (Boal and Rao 1992b). The transition from open to closed topology is found to persist even in the limit of vanishing bending rigidity, where it occurs at a reduced tension $\lambda_e\sigma_0$ of order unity (Boal and Rao 1992b). The reason is again the extra entropy of the boundary fluctuations.

5. Models of hexatic membranes

The crystalline phase of flat membranes is stable because both the energy and entropy of dislocations increases logarithmically with system size (Nelson 1983). With increasing temperature, the free energy of dislocations decreases until there is either a continuous transition to a hexatic phase with short-range translational but quasi-long-ranged bond-orientational order or a first-order transition directly to the fluid phase. This situation changes when the membrane is allowed to buckle out of the plane (Nelson 1996). Seung and Nelson (1988) have shown—by minimizing the energy of a dislocation in a network model of elastic springs—that the energy of dislocations is so reduced by buckling that their energy grows sub-logarithmically with system size. Free dislocations are therefore expected to be present at any finite temperature, destroying the crystalline order.

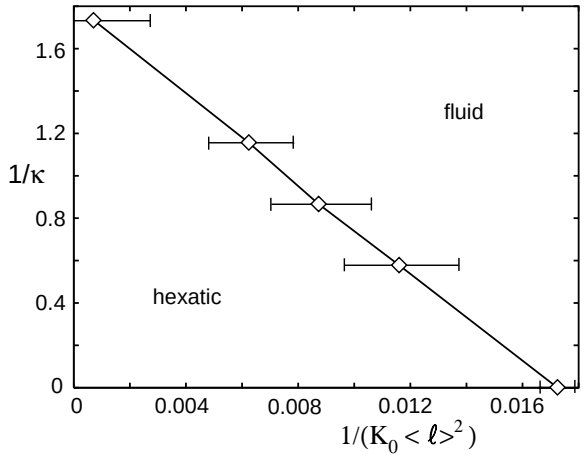

Figure 10. The phase diagram in the $(1/\kappa – 1/[K_0\langle\ell\rangle^2])$ plane, where K_0 is the Young modulus of a polymerized membrane of the same tether length, and $\langle\ell\rangle \simeq (1 + \ell_0)/2$ is the average nearest-neighbour distance. From Gompper and Kroll (1997).

This picture has been confirmed recently by a Monte Carlo simulation of the tether-and-bead model (Gompper and Kroll 1997). In this model, crystalline order is induced by reducing the tether length ℓ_0. The theoretical prediction for the hexatic phase diagram in the $(1/\kappa – 1/K_H)$ plane is shown in figure 2. Because there are as yet no good simulation estimates for the hexatic stiffness, K_H, the phase diagram obtained from simulations is plotted in the $(1/\kappa – 1/[K_0\langle\ell\rangle^2])$ plane in figure 10, where $\langle\ell\rangle$ is the average nearest-neighbour distance, and the fit (Gompper and Kroll 1997)

$$K_0 = 11.33(\ell_0 - 1)^{-2}\left[1 - 2.1\left(\frac{\ell_0 - 1}{\ell_0 + 1}\right)^2\right] \tag{76}$$

has been used for the Young modulus, K_0, of the planar network. A hexatic phase is found for small tether length and sufficiently large bending rigidities $\kappa \gtrsim 1$, in agreement with the predictions of Seung and Nelson (1988). A phase transition to a fluid phase occurs either with increasing tether length or with decreasing bending rigidity, in qualitative agreement with analytic results of Guitter and Kardar (1990) and Park and Lubensky (1996c).

6. Heterogeneous polymer–fluid networks

Heterogeneous membranes, which are composite fluid-polymerized networks, have unusual elastic properties. A prominent example of this type of network is the cell membrane of mammalian red blood cells (Elgsaeter *et al* 1986, Steck 1989). This membrane consists of a lipid bilayer with an attached quasi-hexagonal network of spectrin tetramers. The lipid membrane provides a large area compression modulus and a high flexibility to bending deformations, while the polymer network provides the stiffness required to recover the biconcave equilibrium shape of the red blood cell after being squeezed through narrow capillaries of only a third of their size. Other examples of heterogeneous networks are partially polymerized sheets of certain phospholipid molecules (Sackmann *et al* 1985).

Several models have been used for the simulations of fluid membranes with attached polymer networks. The first study of this problem (Boal *et al* 1992) employs the model of fluid membranes described in section 4.1. In addition to the 'fluid' tethers, a second set of connections is introduced on a small subset of vertices (one in every 36), which form a hexagonal network of fixed connectivity. These 'spectrin' tethers have a maximum length s_{max}, which is the main model parameter. Spectrin tethers are allowed to intersect, as they only represent the in-plane projections of the three-dimensional polymer chains. Monte Carlo simulations of this model show (Boal *et al* 1992) that the dimensionless area compression modulus $K_A\sigma_0^2$ decreases with increasing s_{max}, but quickly reaches a plateau for $s_{max} \gtrsim 8\sigma_0$. The area compression modulus for large s_{max} is therefore mainly determined by the fluid component. The shear modulus, on the other hand, is found to decrease rapidly with increasing s_{max}; it is determined by the polymer network. Furthermore, the Poisson ratio σ_P of the spectrin network was shown to be *negative*. Such materials expand transversely when stretched longitudinally. Note that no out-of-plane fluctuations of the membrane are taken into account in this model. Thus, the physical mechanism for $\sigma_P < 0$ must be *different* from the case discussed in sections 2.1.8 and 3.2.1 above.

To get more insight into this unexpected result, a simplified model has been considered (Boal *et al* 1993). In this case, the fluid component is not taken into account explicitly, but only via a lateral tension on the spectrin network which determines the average area per vertex. The interaction was taken to be either a square-well potential or Hookean springs, and both self-avoiding and phantom membranes were examined. In all of these cases, a *negative* Poisson ratio was found over some range of the lateral tension.

Finally, the polymeric nature of the spectrin network has been taken into account explicitly (Boal 1994). In this case, the bonds in the hexagonal network are replaced by short polymer chains, with chain lengths in the range 4–30 (compare section 3.2.3). The midpoint of each chain is then constrained to move in a plane which represents the bilayer. This plane acts as a repulsive hard wall to all other segments. This model has been used to calculate the elastic moduli of red-blood-cell membranes (Boal 1994).

Networks, in which a fraction p of randomly selected bonds are polymerized, have also been studied (Boal 1993). It is found that the area compression modulus K_A is essentially independent of the polymer fraction p. On the other hand, the shear modulus vanishes below the percolation threshold p_c, and increases roughly linearly with p for $p > p_c$.

7. Plaquette and triangular lattice models

7.1. Plaquette models

Plaquette models are surfaces which are composed of connected faces of elementary cells of a cubic lattice. The surface can be defined, for example, by introducing a spin variable $s_i \in \{-1, 1\}$ in each cell. The surface is then given by those faces which separate cells of opposite spin. Such plaquette surfaces are always closed. However, open surfaces can also be studied by using other variables to describe the surface positions. Self-intersections are possible on a simple cubic lattice—although they can be avoided by introducing extra terms in the Hamiltonian, of course—but do not occur on a body-centred cubic lattice (Dotsenko *et al* 1993). Plaquette models have been investigated with bending rigidity, i.e. with an energy contribution which favours the parallel alignment of neighbouring plaquettes. However, it should be emphasized that it is extremely difficult to discretize the squared mean curvature on a lattice correctly. The scale invariance of the curvature Hamiltonian is therefore usually broken in plaquette models (Likos *et al* 1995).

Surfaces on cubic lattices are outside of the main focus of this review. The most important theoretical results concerning lattice plaquette models are reviewed by Fröhlich (1985). We want to provide here only a short summary of relevant simulation results. Vesicles and open membranes without bending rigidity have been studied in considerable detail. The most detailed investigations of branched polymer behaviour have been performed with the use of plaquette models (Glaus 1986, 1988, O'Connell *et al* 1991, Baumgärtner and Renz 1992). Vesicles with fluctuating genus have also been considered. It has been shown (Stella *et al* 1992) that the fluctuating topology does not change the universality class, in agreement with the result of network models mentioned above. This corrects earlier results in which a different scaling behaviour had been observed (Banavar *et al* 1991). Several simulations of lattice vesicles with a pressure difference between inside and outside (Orlandini and Tesi 1992, Baumgärtner 1992) or with constant enclosed volume (Baumgärtner 1993b) have been carried out. The results are similar to those obtained from network models; compare section 4.3 above. However, the transition pressure p^* of the branched-to-inflated transition was found to scale as $N^{-\zeta_+}$ with $\zeta_+ = 1$, in contrast to $\zeta_+ \leqslant 0.7$ for network models (compare section 4.3).

The main disadvantage of plaquette models is that the bending energy cannot easily be discretized on a cubic lattice. This can be seen most easily by considering the scale invariance of the continuum curvature Hamiltonian: the curvature energy of a sphere is $4\pi(2\kappa + \bar{\kappa})$, *independent* of the vesicle radius. All naive discretizations on cubic lattices, where the analogue of a sphere is a cube, lead to a *linear* dependence of the discretized curvature energy on the cube size (Likos *et al* 1995). Thus, the results for plaquette models

for large bending rigidities (Baumgärtner 1993a, Orlandini *et al* 1996) have to be interpreted very carefully.

Finally we want to mention the study of vesicle adsorption in the case of zero bending rigidity (Orlandini *et al* 1993).

7.2. Folding transitions

A very simple model in $d = 2$ dimensions which has some of the properties of tethered networks has been suggested by David and Guitter (1988). It was originally formulated on a square lattice. The elementary squares of the lattice are rigid, so the only degrees of freedom are folds along the lines of the lattice. They showed that the entropy of this model is not extensive, so for any finite bending energy, the surface is flat, with $d_f = 2$. There is a folding transition at zero bending rigidity, where the surface has the fractal dimension $d_f = 4$. A similar model on a triangular lattice exhibits more interesting behaviour (Kantor and Jarić 1990, Di Francesco and Guitter 1994a, b). In particular, the entropy per site is finite (Kantor and Jarić 1990, Di Francesco and Guitter 1994a), and there is a first-order folding transition at a finite value of the bending rigidity (Di Francesco and Guitter 1994b). This folding transition is closely related to the crumpling transition in $d = 2$ dimensions studied by Renken and Kogut (1991a) (see section 3.2.2); the only difference between the models is that in the present case, the sides of the elementary triangles have fixed length, while in the model considered by Renken and Kogut (1991a), they are allowed to fluctuate. Bowick *et al* (1995) have determined the folding entropy per surface triangle for a model of three-dimensional folding, where folds are allowed to be either planar or form the angles of a regular octahedron. Di Francesco *et al* (1997) have used the cluster variation method to determine the folding phase diagram of the regular triangular lattice in the presence of a quenched random bending rigidity $\pm\kappa$ and magnetic field conjugate to the local normal vectors of the surface triangles. Folding of the triangular lattice in three dimensions with *negative* bending rigidity (Bowick *et al* 1997), and of the square lattice in two dimensions with bending rigidity and attractive or repulsive interactions (Mori and Kajinaga 1996) has also been studied.

8. Outlook

There has been enormous progress in the understanding of the thermal behaviour of simple, one-component membranes over the last few years. This is due, in part, to the fruitful interaction between theory and computer simulations.

Nevertheless, several questions require further analysis. We give just a few examples. First, the existence of a crumpled phase for *polymerized*, self-avoiding membranes with attractive interactions has to be demonstrated more convincingly. Also, the dependence of the stability of a crumpled phase on the range and strength of the attractive interaction has to be investigated systematically. Second, the effect of the boundary fluctuations (Abraham and Nelson 1990b, Gompper and Kroll 1992a) on polymerized membranes with free edges has to be better understood, since the origin of the small but significant difference between the values for the exponents ζ and η obtained from simulations of open and closed membranes still remains unclear. Third, for *fluid* membranes, the existence of a phase transition with increasing bending rigidity is still unclear. The existence of such a transition would have important consequences for the renormalization of the bending rigidity, since it would indicate that the softening of the membrane by thermal fluctuations has to change into a stiffening at very large length scales (Bowick *et al* 1993). Finally, the scaling behaviour of

low-bending-rigidity vesicles at the branched-to-inflated transition has to be investigated in more detail.

With the behaviour of simple systems now relatively well understood, simulation methods will certainly be applied in the near future to more complex systems. The simulation of membranes of fluctuating topology, for example, will help to answer many important questions, such as the form of the vesicle size distribution (Morse and Milner 1995), the shape of the lamellar-to-sponge phase boundary (Morse 1994, Golubovič 1994), and the density of passages in the lamellar phase (Golubovič 1994, Gompper and Goos 1995). In particular, this should give access to the renormalization of the saddle-splay modulus. The thermal behaviour of heterogeneous membranes, such as membranes composed of two lipid components, membranes decorated with anchored polymers, or membranes with embedded proteins, plays an important role in all biomembranes (Lipowsky 1995, Goulian 1995, Lasic and Papahadjopoulos 1995). Simulations will be an important tool in efforts to understand the interplay between shape and aggregation, which plays an essential role in the biological functioning of a membrane.

References

Abraham F F 1991 *Phys. Rev. Lett.* **67** 1669

——1992 *Microscopic Simulations of Complex Hydrodynamic Phenomena* ed M Mareschal and B L Holian (New York: Plenum) p 361

Abraham F F and Goulian M 1992 *Europhys. Lett.* **19** 293

Abraham F F and Kardar M 1991 *Science* **252** 419

Abraham F F and Nelson D R 1990a *Science* **249** 393

——1990b *J. Physique* **51** 2653

Abraham F F, Rudge W E and Plischke M 1989 *Phys. Rev. Lett.* **62** 1757

Alexander S 1982 *J. Physique Lett.* **43** L625

Ambjørn J, Białas P, Burda Z, Jurkiewicz J and Petersson B 1995a *Phys. Lett.* **342B** 58

Ambjørn J, Białas P, Jurkiewicz J, Burda Z and Petersson B 1994 *Phys. Lett.* **325B** 337

Ambjørn J, Burda Z, Jurkiewicz J and Petersson B 1995b *Phys. Lett.* **341B** 286

Ambjørn J, Durhuus B and Fröhlich J 1985 *Nucl. Phys.* B **257** 433

Ambjørn J, Durhuus B and Jonsson T 1989 *Nucl. Phys.* B **316** 526

Ambjørn J, Irbäck A, Jurkiewicz J and Petersson B 1993 *Nucl. Phys.* B **393** 571

Ambjørn J, Jurkiewicz J and Watabiki Y 1995c *Nucl. Phys.* B **454** 313

Ammann A and Lipowsky R 1996 *J. Physique* II **6** 255

Anagnostopoulos K, Bowick M, Coddington P, Falcioni M, Han L, Harris G and Marinari E 1993 *Phys. Lett.* **317B** 102

Aronowitz J A, Golubović L and Lubensky T C 1989 *J. Physique* **50** 609

Aronowitz J A and Lubensky T C 1987 *Europhys. Lett.* **4** 395

——1988 *Phys. Rev. Lett.* **60** 2634

Baig M, Espriu D and Travesset A 1994 *Nucl. Phys.* B **426** 575

Baig M, Espriu D and Wheater J F 1989a *Nucl. Phys.* B **314** 609

——1989b *Nucl. Phys.* B **314** 587

Baillie C F and Johnston D A 1992 *Phys. Lett.* **283B** 55

Baillie C F, Johnston D A and Williams R D 1990 *Nucl. Phys.* B **335** 469

Baillie C F, Williams R D, Catterall S M and Johnston D A 1991 *Nucl. Phys.* B **348** 543

Banavar J R, Maritan A and Stella A 1991 *Science* **252** 825

Barsky S J and Plischke M 1994 *Phys. Rev.* E **50** 3911

Baumgärtner A 1991 *J. Physique* I **1** 1549

——1992 *Physica* A **190** 63

——1993a *Physica* A **192** 550

——1993b *J. Chem. Phys.* **98** 7496

Baumgärtner A and Ho J S 1990 *Phys. Rev.* A **41** 5747

Baumgärtner A and Renz W 1992 *Europhys. Lett.* **17** 381

Baumgärtner A and Romero A 1992 *Physica* A **187** 243

Bensimon D, Mukamel D and Peliti L 1992 *Europhys. Lett.* **18** 269
Billoire A and David F 1986 *Nucl. Phys.* B **275** 617
Billoire A, Gross D J and Marinari E 1984 *Phys. Lett.* **139B** 75
Bloom M, Evans E and Mouritsen O G 1991 *Q. Rev. Biophys.* **24** 293
Boal D H 1993 *Phys. Rev.* E **47** 4604
——1994 *Biophys. J.* **67** 521
Boal D H, Levinson E, Liu D and Plischke M 1989 *Phys. Rev.* A **40** 3292
Boal D H and Rao M 1992a *Phys. Rev.* A **45** R6947
——1992b *Phys. Rev.* A **46** 3037
Boal D H, Seifert U and Shillcock J C 1993 *Phys. Rev.* E **48** 4274
Boal D H, Seifert U and Zilker A 1992 *Phys. Rev. Lett.* **69** 3405
Boulatov D V, Kazakov V A, Kostov I K and Migdal A A 1986 *Nucl. Phys.* B **275** 641
Bowick M, Coddington P, Han L, Harris G and Marinari E 1993 *Nucl. Phys.* B **394** 791
Bowick M J, Catterall S M, Falcioni M, Thorleifsson G and Anagnostopoulos K N 1996 *J. Physique* I **6** 1321
Bowick M J, Di Francesco P, Golinelli O and Guitter E 1995 *Nucl. Phys.* B **450** 463
Bowick M J, Golinelli O, Guitter E and Mori S 1997 *Nucl. Phys.* B **495** 583
Cai W, Lubensky T C, Nelson P and Powers T 1994 *J. Physique* II **4** 931
Camacho C J, Fisher M E and Singh R R P 1991 *J. Chem. Phys.* **94** 5693
Canham P B 1970 *J. Theor. Biol.* **26** 61
Cates M E 1984 *Phys. Rev. Lett.* **53** 926
Catterall S M 1989 *Phys. Lett.* **220B** 207
Ceperley D, Kalos M H and Lebowitz J L 1978 *Phys. Rev. Lett.* **41** 313
Cevc G, Blume G, Schätzlein A, Gebauer D and Paul A 1996 *Adv. Drug Delivery Rev.* **18** 349
Cook-Röder J and Lipowsky R 1992 *Europhys. Lett.* **18** 433
Dammann B, Fogeby H C, Ipsen J H and Jeppesen C 1994 *J. Physique* I **4** 1139
David F 1989 *Statistical Mechanics of Membranes and Surfaces* ed D Nelson, T Piran and S Weinberg (Singapore: World Scientific) pp 157–223
David F, Ginsparg P and Zinn-Justin J (ed) 1996 *Fluctuating Geometries in Statistical Mechanics and Field Theory* (Amsterdam: Elsevier)
David F and Guitter E 1988 *Europhys. Lett.* **5** 709
David F, Guitter E and Peliti L 1987 *J. Physique* **48** 2059
David F and Leibler S 1991 *J. Physique* II **1** 959
Deem M W and Nelson D R 1996 *Phys. Rev.* E **53** 2551
de Gennes P-G 1974 *J. Chem. Phys.* **60** 5030
Di Francesco P and Guitter E 1994a *Europhys. Lett.* **26** 455
——1994b *Phys. Rev.* E **50** 4418
Di Francesco P, Guitter E and Mori S 1997 *Phys. Rev.* E **55** 237
Dotsenko V S, Windey P, Harris G, Marinari E, Martinec E and Picco M 1993 *Phys. Rev. Lett.* **71** 811
Duering E and Kantor Y 1989 *Phys. Rev.* B **40** 7443
Duplantier B 1987 *Phys. Rev. Lett.* **58** 2733
Duwe H P, Käs J and Sackmann E 1990 *J. Physique* **51** 945
Elgsaeter A, Stokke B T, Mikkelsen A and Branton D 1986 *Science* **234** 1217
Espriu D 1987 *Phys. Lett.* **194B** 271
Espriu D and Travesset A 1995 *Phys. Lett.* **356B** 329
——1996 *Nucl. Phys. (Proc. Suppl.)* B **47** 637
Evans E A 1974 *Biophys. J.* **14** 923
Falcioni M, Bowick M J, Guitter E and Thorleifsson G 1997 *Europhys. Lett.* **38** 67
Förster D 1986 *Phys. Lett.* **114A** 115
Fröhlich J 1985 *Applications of Field Theory to Statistical Mechanics (Springer Lecture Notes in Physics 216)* ed L Garido (Berlin: Springer) p 32
Gefen Y, Aharony A and Alexander S 1983 *Phys. Rev. Lett.* **50** 77
Gefen Y, Aharony A, Mandelbrot B B and Kirkpatrick S 1981 *Phys. Rev. Lett.* **47** 1771
Gelbart W M, Ben-Shaul A and Roux D (ed) 1995 *Micelles, Membranes, Microemulsions, and Monolayers* (Berlin: Springer)
Glaus U 1986 *Phys. Rev. Lett.* **56** 1996
——1988 *J. Stat. Phys.* **50** 1141
Golubovič L 1994 *Phys. Rev.* E **50** R2419
Gompper G and Goos J 1994 *Phys. Rev.* E **50** 1325

——1995 *J. Physique* II **5** 621
Gompper G and Kroll D M 1989 *Europhys. Lett.* **9** 59
——1991a *J. Physique* I **1** 1411
——1991b *Europhys. Lett.* **15** 783
——1992a *J. Physique* I **2** 663
——1992b *Europhys. Lett.* **19** 581
Gompper G and Kroll D M 1992c *Phys. Rev.* A **46** 7466
——1993 *Phys. Rev. Lett.* **71** 1111
——1994 *Phys. Rev. Lett.* **73** 2139
——1995a *Phys. Rev.* E **52** 4198
——1995b *Phys. Rev.* E **51** 514
——1996 *J. Physique* I **6** 1305
——1997 *Phys. Rev. Lett.* **78** 2859
Gompper G and Schick M 1994 *Phase Transitions and Critical Phenomena* vol 16, ed C Domb and J Lebowitz (London: Academic) pp 1–176
Goulian M 1991 *J. Physique* II **1** 1327
——1995 *Curr. Opin. Colloid Interface Sci.* **1** 358
Goulian M, Lei N, Miller J and Sinha S K 1992 *Phys. Rev.* A **46** R6170
Grest G S 1991 *J. Physique* I **1** 1695
Grest G S and Murat M 1990 *J. Physique* I **51** 1415
——1995 *Monte Carlo and Molecular Dynamics Simulations in Polymer Sciences* ed K Binder (New York: Oxford University Press)
Grest G S and Petsche I B 1994 *Phys. Rev.* E **50** R1737
Gross D J 1984 *Phys. Lett.* **139B** 187
Guitter E, David F, Leibler S and Peliti L 1988 *Phys. Rev. Lett.* **61** 2949
——1989 *J. Physique* **50** 1787
Guitter E and Kardar M 1990 *Europhys. Lett.* **13** 441
Guitter E, Leibler S, Maggs A C and David F 1990 *J. Physique* **51** 1055
Guitter E and Palmeri J 1992 *Phys. Rev.* A **45** 734
Halperin B I and Nelson D R 1978 *Phys. Rev. Lett.* **41** 121
Harnish R G and Wheater J F 1991 *Nucl. Phys.* B **350** 861
Havlin S, Djordjevic Z V, Majid I, Stanley H E and Weis G H 1984 *Phys. Rev. Lett.* **53** 178
Heinrich V, Sevšek F, Svetina S and Žekš B 1997 *Phys. Rev.* E **55** 1809
Helfrich W 1973 *Z. Naturf.* c **28** 693
——1974 *Phys. Lett.* **50A** 115
——1978 *Z. Naturf.* a **33** 305
——1985 *J. Physique* **46** 1263
——1986 *J. Physique* **47** 321
——1990 *Liquids at Interfaces, Les Houches Session XLVIII (1988)* ed J Charvolin, J F Joanny and J Zinn-Justin (Amsterdam: Elsevier)
Ho J S and Baumgärtner A 1989 *Phys. Rev. Lett.* **63** 1324
——1990 *Europhys. Lett.* **12** 295
Hwa T 1990 *Phys. Rev.* A **41** 1751
Ipsen J H and Jeppesen C 1995 *J. Physique* I **5** 1563
Israelachvili J N 1992 *Intermolecular and Surface Forces* (London: Academic)
Itzykson C 1986 *Proc. GIFT Seminar, Jaca 85* ed J Abad, M Asorey and A Cruz (Singapore: World Scientific) pp 130–88
Janke W, Kleinert H and Meinhard M 1989 *Phys. Lett.* **217B** 525
Jeppesen C and Ipsen J H 1993 *Europhys. Lett.* **22** 713
Jülicher F 1994 Die Morphologie von Vesikeln *PhD Thesis* Universität zu Köln
Kantor Y 1992 *Europhys. Lett.* **20** 337
Kantor Y and Jarić M V 1990 *Europhys. Lett.* **11** 157
Kantor Y, Kardar M and Nelson D R 1986 *Phys. Rev. Lett.* **57** 791
——1987 *Phys. Rev.* A **35** 3056
Kantor Y and Kremer K 1993 *Phys. Rev.* E **48** 2490
Kantor Y and Nelson D R 1987a *Phys. Rev. Lett.* **58** 2774
——1987b *Phys. Rev.* A **36** 4020
Kardar M and Nelson D R 1987 *Phys. Rev. Lett.* **58** 1289

Kazakov V A, Kostov I K and Migdal A A 1985 *Phys. Lett.* **157B** 295
Kleinert H 1986 *Phys. Lett.* **114A** 263
Komura S and Baumgärtner A 1990 *J. Physique* **51** 2395
Kosterlitz J M and Thouless D J 1973 *J. Phys. C: Solid State Phys.* **6** 1181
Kramer E M and Witten T A 1997 *Phys. Rev. Lett.* **78** 1303
Kraus M, Wintz W, Seifert U and Lipowsky R 1996 *Phys. Rev. Lett.* **77** 3685
Kroll D M and Gompper G 1992a *Science* **255** 968
——1992b *Phys. Rev.* A **46** 3119
——1993 *J. Physique* I **3** 1131
——1995 *J. Chem. Phys.* **102** 9109
Kumar P B S and Rao M 1996 *Mol. Cryst. Liq. Cryst.* **288** 105
Lamb L D, Huffman D R, Workman R K, Howells S, Chen T, Sarid D and Ziolo R F 1992 *Science* **255** 1413
Lasic D D and Papahadjopoulos D 1995 *Science* **267** 1275
Le Doussal P 1992 *J. Phys. A: Math. Gen.* **25** L469
Le Doussal P and Radzihovsky L 1992 *Phys. Rev. Lett.* **69** 1209
——1993 *Phys. Rev.* B **48** 3548
Leibler S and Maggs A C 1989 *Phys. Rev. Lett.* **63** 406
Levinson E 1991 *Phys. Rev.* A **43** 5233
Likos C N, Mecke K R and Wagner H 1995 *J. Chem. Phys.* **102** 9350
Lipowsky R 1991 *Nature* **349** 475
——1995 *Curr. Opin. Struct. Biol.* **5** 531
Lipowsky R and Giradet M 1990 *Phys. Rev. Lett.* **65** 2893
Lipowsky R and Leibler S 1986 *Phys. Rev. Lett.* **56** 2541
Lipowsky R and Sackmann E (ed) 1995 Structure and dynamics of membranes—from cells to vesicles *Handbook of Biological Physics* vols 1A, 1B (Amsterdam: Elsevier)
Lipowsky R and Zielinska B 1989 *Phys. Rev. Lett.* **62** 1572
Litster J D 1975 *Phys. Lett.* **53A** 193
Liu D and Plischke M 1992 *Phys. Rev.* A **45** 7139
Lobkovsky A 1996 *Phys. Rev.* E **53** 3750
Lobkovsky A, Gentges S, Li H, Morse D and Witten T A 1995 *Science* **270** 1482
Lobkovsky A and Witten T A 1997 *Phys. Rev.* E **55** 1577
Maggs A C, Leibler S, Fisher M E and Camacho C J 1990 *Phys. Rev.* A **42** 691
Milner S T and Safran S A 1987 *Phys. Rev.* A **36** 4371
Mori S 1996a *J. Phys. Soc. Japan* **65** 1988
——1996b *Phys. Rev.* E **54** 338
Mori S and Kajinaga Y 1996 *Phys. Rev.* E **53** 124
Mori S and Wadati M 1994 *Phys. Rev.* E **50** 867
Morse D C 1994 *Phys. Rev.* E **50** R2423
Morse D C and Lubensky T C 1992 *Phys. Rev.* A **46** 1751
Morse D C, Lubensky T C and Grest G S 1992a *Phys. Rev.* A **45** R2151
Morse D C and Milner S T 1995 *Phys. Rev.* E **52** 5918
Morse D C, Petsche I B, Grest G S and Lubensky T C 1992b *Phys. Rev.* A **46** 6745
Münkel C and Heermann D W 1992 *J. Physique* I **2** 2181
——1993 *J. Physique* I **3** 1359
——1995 *Phys. Rev. Lett.* **75** 1666
Nelson D, Piran T and Weinberg S (ed) 1989 *Statistical Mechanics of Membranes and Surfaces* (Singapore: World Scientific)
Nelson D R 1983 *Phase Transitions and Critical Phenomena* vol 7, ed C Domb and J Lebowitz (London: Academic) pp 1–99
——1989 *Statistical Mechanics of Membranes and Surfaces* ed D Nelson, T Piran and S Weinberg (Singapore: World Scientific) pp 137–55
——1996 *Fluctuating Geometries in Statistical Mechanics and Field Theory* ed F David, P Ginsparg and J Zinn-Justin (Amsterdam: North-Holland) pp 423–77
Nelson D R and Peliti L 1987 *J. Physique* **48** 1085
Nelson D R and Radzihovsky L 1991 *Europhys. Lett.* **16** 79
Netz R R 1995 *Phys. Rev.* E **52** 1897
Netz R R and Lipowsky R 1993 *Phys. Rev. Lett.* **71** 3596
——1995 *Europhys. Lett.* **29** 345

O'Connell J, Sullivan F, Libes D, Orlandini E, Tesi M C, Stella A L and Einstein T L 1991 *J. Phys. A: Math. Gen.* **24** 4619
Orlandini E, Stella A L, Einstein T L, Tesi M C, Beichl I and Sullivan F 1996 *Phys. Rev.* E **53** 5800
Orlandini E, Stella A L, Tesi M C and Sullivan F 1993 *Phys. Rev.* E **48** R4203
Orlandini E and Tesi M C 1992 *Physica* A **185** 160
Paczuski M, Kardar M and Nelson D R 1988 *Phys. Rev. Lett.* **60** 2638
Park J M and Lubensky T C 1996a *J. Physique* I **6** 493
——1996b *Phys. Rev.* E **53** 2665
——1996c *Phys. Rev.* E **53** 2648
Peliti L and Leibler S 1985 *Phys. Rev. Lett.* **54** 1690
Peter U, König S, Roux D and Bellocq A M 1996 *Phys. Rev. Lett.* **76** 3866
Petsche I B and Grest G S 1993 *J. Physique* I **3** 1741
Plischke M and Fourcade B 1991 *Phys. Rev.* A **41** 2056
Polyakov A M 1986 *Nucl. Phys.* B **286** 406
Radzihovsky L and Le Doussal P 1992 *J. Physique* I **2** 599
Radzihovsky L and Nelson D R 1991 *Phys. Rev.* A **44** 3525
Renken R L and Kogut J B 1990 *Nucl. Phys.* B **342** 753
——1991a *Nucl. Phys.* B **350** 554
——1991b *Nucl. Phys.* B **354** 328
Sackmann E, Eggl P, Fahn C, Bader H, Ringsdorf H and Schollmeier M 1985 *Ber. Bunsenges. Phys. Chem.* **89** 1198
Safinya C R, Roux D, Smith G S, Sinha S K, Dimon P, Clark N A and Bellocq A M 1986 *Phys. Rev. Lett.* **57** 2718
Schmidt C F, Svoboda K, Lei N, Petsche I B, Berman L E, Safinya C R and Grest G S 1993 *Science* **259** 952
Seifert U 1995 *Z. Phys.* B **97** 299
——1997 *Adv. Phys.* **46** 13
Seifert U, Berndl K and Lipowsky R 1991 *Phys. Rev.* A **44** 1182
Seung H S and Nelson D R 1988 *Phys. Rev.* A **38** 1005
Shillcock J C and Boal D H 1996 *Biophys. J.* **71** 317
Spector M S, Naranjo E, Chiruvolu S and Zasadzinski J A 1994 *Phys. Rev. Lett.* **73** 2867
Steck T L 1989 *Cell Shape: Determinants, Regulation, and Regulatory Role* ed W Stein and F Bonner (New York: Academic) pp 205–46
Stella A L, Orlandini E, Beichl I, Sullivan F, Tesi M C and Einstein T L 1992 *Phys. Rev. Lett.* **69** 3650
Strey R, Schomäcker R, Roux D, Nallet F and Olsson U 1990 *J. Chem. Soc. Faraday Trans.* **86** 2253
Tanford C 1980 *The Hydrophobic Effect: Formation of Micelles and Biological Membranes* 2nd edn (New York: Wiley)
Taniguchi T 1996 *Phys. Rev. Lett.* **76** 4444
van de Ven T G M 1989 *Colloidal Hydrodynamics* (London: Academic)
Wen X, Garland C W, Hwa T, Kardar M, Kokufuta E, Li Y, Orkisz M and Tanaka T 1992 *Nature* **355** 426
Wheater J F 1994 *J. Phys. A: Math. Gen.* **27** 3323
——1996 *Nucl. Phys.* B **458** 671
Wheater J F and Stephenson P W 1993 *Phys. Lett.* **302B** 447
Witten T A and Li H 1993 *Europhys. Lett.* **23** 51
Young A P 1979 *Phys. Rev.* B **19** 1855
Zhang Z, Davis H T and Kroll D M 1993 *Phys. Rev.* E **48** R651
——1996 *Phys. Rev.* E **53** 1422
Zhang Z, Davis H T, Maier R S and Kroll D M 1995 *Phys. Rev.* B **52** 5404